ELSEVIER

Journal of Fluids and Structures 24 (2008) 954–976

JOURNAL OF FLUIDS AND STRUCTURES

www.elsevier.com/locate/jfs

# Dynamics of trains and train-like articulated systems travelling in confined fluid—Part 2: Wave propagation and flow-excited vibration

Y. Sakuma*, M.P. Païdoussis, S.J. Price

*Department of Mechanical Engineering, McGill University, 817 Sherbrooke Street West, Montreal, Québec, Canada H3A 2K6*

Received 24 October 2006; accepted 5 January 2008
Available online 7 May 2008

**Abstract**

Wave propagation and response of a train of flexibly interconnected rigid cars travelling in a confined cylindrical "tunnel" subjected to fluid dynamic forces are studied theoretically. For the wave propagation analysis, an infinite-length train represented by a lumped-parameter Timoshenko-beam (LTB) model is employed. The train response is simulated using a travelling sinusoidal aerodynamic force that mimics the features obtained during running experiments on real trains. In addition, the response of the system is examined when the velocity of the force approaches the minimum phase velocity of a travelling wave in the train. The principal aim of this study is to investigate the effect of aerodynamic forces on the dynamics of a high-speed train running in a tunnel, or more generally of a train-like system travelling in a coaxial cylindrical tube. The results of this study show that: (a) when aerodynamic forces act on a train, the frequency bands of the dispersion relation of wave propagation shift, and thus no classical normal modes (standing wave solutions) exist in the system; (b) the wavelength of the travelling sinusoidal force controls the phase differences between cars in the train; and (c) the response of the train can be considerably amplified when the speed of the travelling force coincides with the minimum phase velocity of travelling waves in the train.


*Keywords:* Trains; Articulated systems; Wave propagation; Aerodynamic forces; Spatially periodic structures; Dispersion relation

## 1. Introduction

Since 1986, fluid–structure interactions of high-speed trains have been studied in Japan as one of the issues affecting ride quality (Sasaki and Shimomura, 1989; Fujimoto and Miyamoto, 1996). As trains travel at higher speeds, the vibration amplitudes become greater, especially in tunnel sections. It has been noted that the yawing and lateral vibration of trains in a tunnel section is more pronounced than when the same train is travelling in the open environment (non-tunnel), and that the vibration amplitude gradually increases from the head toward the tail of a train. Initially, track irregularity was supposed to be a major cause of the vibrations, but little correlation between track

*Corresponding author. Present address: Railway Technical Research Institute, Aerodynamics Laboratory, 2-8-38 Hikari-cho, Kokubunji-shi, Tokyo 185-8540, Japan.
*E-mail address:* sakuma@rtri.or.jp (Y. Sakuma).

0889-9746/$ - see front matter © 2008 Elsevier Ltd. All rights reserved.
doi:10.1016/j.jfluidstructs.2008.01.003

irregularity and the vibrations was found for trains travelling in tunnels; this indicated that track irregularity was not the cause of the vibrations (Takai, 1989).

A mechanism for the vibrations based on aerodynamic effects of the tail car was proposed by Suzuki et al. (1996). However, the aerodynamic forces on intermediate cars were not considered. Later, the effect of aerodynamic forces acting on intermediate cars was investigated (Ishihara et al., 1997; Sakuma et al., 1998; Ueki et al., 1999). Vibrations and pressure fluctuations on the sides of a car were measured simultaneously, both in the open and in tunnel sections, and aerodynamic forces on the car were calculated from the pressure data. It was found that: (i) the aerodynamic force in tunnel sections is much greater than that in the open; (ii) the aerodynamic force and the vibration in tunnel sections gradually increases from the head toward the tail of the train; and (iii) lateral and yawing vibrations of the car have a close correlation with the aerodynamic forces acting on the car. Velocity and pressure fluctuations on the sides of a high-speed train were also measured simultaneously, using hot-film probes and pressure gauges, by Sakuma et al. (1998). A strong correlation between pressure and velocity fluctuations indicated the existence of large-scale coherent structures moving downstream at a speed equivalent to about 80% of the train speed.

Numerical simulations and wind tunnel experiments for the flow around a high-speed train travelling in a tunnel have been conducted by several researchers (Suzuki, 2001; Suzuki et al., 2001, 2002; Nakade et al., 2004). These investigations indicated that the flow on the sides of intermediate cars of a high-speed train contains vortical structures generated near the under-corners of those cars facing the tunnel wall. It was also shown that these vortices are responsible for the pressure fluctuations. Fixing fins on the under-corners of the car bodies has been proposed as a means of reduction of the aerodynamic force acting on the sides of the cars (Suzuki, 2001). An analytical model representing the pressure fluctuations travelling along the side of a *single* car in a train has been proposed by Suzuki (1999). The pressure fluctuations were assumed to be a sinusoidal travelling wave function, which resulted in a lateral force and a yawing moment acting on the car; however, the dynamics of the car were not studied.

Fujimoto et al. (1998) measured the vibrations on two adjacent cars of a Japanese high-speed train, both in the open and in tunnel sections, and calculated the phase difference between the vibration of these cars. It was found that, for trains in a tunnel, both lateral and yawing motion of the back car lead those of the front car by 90°. This was not observed when the train was travelling in the open. In addition, they monitored the motion of five adjacent cars over a period of vibration; with increasing time, for trains travelling in a tunnel, motion of the back car was found to propagate to the front car. The cause of this motion, however, was not clarified.

Trains and train-like articulated systems consist of a chain of cars with similar mechanical properties, and consequently they can be considered as a periodic structure. When vibrations propagate as waves in periodic structures, waves within specific frequency bands can travel freely, while others are attenuated. The velocities of wave propagation vary with frequency, as defined by a ''dispersion relation'' which is determined by the nature and configuration of the system. The analysis of wave propagation by means of the dispersion relation is a valuable tool in understanding the dynamics of periodic structures.

To the authors' knowledge, very little work on wave propagation in trains has been reported. The theory of aeroelastic wave propagation along an infinitely long beam travelling in an air-filled tunnel lined with Helmholtz resonators was developed by Sugimoto (1996), who also examined the effect of the lining on the stability of the beam. Flexural wave propagation in a spatially periodic structure of articulated beams was studied by Sugimoto et al. (2002) and Watanabe and Sugimoto (2003, 2005). These papers considered flexural wave propagation in a spatially periodic structure consisting of identical beams of finite length, connected to adjoining ones by couplers giving restoring moment at the junctions. Wave propagation in an infinite-length train of coupled rigid bodies mounted on elastic supports in a vacuum was studied by Manabe (2002). Manabe showed that waves can propagate freely in an infinite-length train in both the positive and negative directions within only two frequency bands (Born and Hunag, 1954). These frequency bands correspond to two different vibrational modes, and their propagation velocities are of the same order of magnitude as the running velocity of high-speed trains. No stability analysis was carried out in Manabe's work.

As shown in Part 1 of this study (Sakuma et al., 2008), the present system can be modelled as a lumped-parameter Timoshenko beam, LTB, on elastic supports in air flow. Thus, the present study may provide a general framework for the discussion of the effects of aerodynamic forces and stiffness configuration on wave propagation in LTB models on elastic supports.

In this study, the theoretical studies of Païdoussis (1986, 2003) and Suzuki (1999), referred to in Part 1 (Sakuma et al., 2008) and in the foregoing, will be employed as the foundation for the investigation of the dynamics of a train in a tunnel. Moreover, we not only employ these earlier studies but also integrate and extend them. Initially, in Section 2, we analyze wave propagation in an infinite-length train of coupled rigid bodies mounted on elastic supports, both in vacuum and in air. Then, in Section 3, we study the response of a finite-length train to a travelling sinusoidal aerodynamic force that simulates the features obtained during running experiments on real trains. In addition, the response of the system is examined when the velocity of the force approaches the minimum phase velocity of the

travelling wave obtained in Section 2. The motivation for this is that it is known that if any one-dimensional or quasi-one-dimensional continuous periodic structure is excited by a harmonic pressure field which is convected along the length of the structure, and if the convection velocity is equal to the phase velocity of one of the free waves in the structure, then that wave will be excited and a large response will occur (Mead, 1971; Manabe, 2002).

Note that the dynamic response of articulated beams to a moving load is somewhat more complicated than that of continuous systems. The complication originates from the fact that in discrete systems each vibration frequency corresponds to infinitely many spatial forms (these are not the physical modes of vibrations but simply motions with different wavelengths). This is in contrast to continuous systems in which only a few (normally one per physical mode) spatial forms correspond to a frequency (Suiker et al., 2001).

The main contribution of this paper is the study of the response and mode shapes of an LTB train of free–free coupled rigid cylinders with elastic supports to a travelling sinusoidal aerodynamic force. This simulates very closely the features of aerodynamic forces obtained in actual running experiments. In particular, the results we obtain, clarifying the mechanism by which the wavelength of the travelling force controls the phase differences between cars in a train, are new.

## 2. Wave propagation in an infinite-length train according to the LTB model

### 2.1. Derivation of the dispersion relation

In this section, the dispersion relation is derived by substituting travelling-wave solutions into the simplified equations of motion.

The dimensionless equations of motion for a train of $N$ identical cars given in Part 1 of this study (Sakuma et al., 2008) are simplified by (i) setting to zero all mechanical damping terms, (ii) omitting the terms for the leading ($j=1$) and trailing ($j=N$) cars; this allows the length of the train be considered as infinite, and (iii) letting $\overline{k}_{fj}=\overline{k}_{bj}=\overline{k}_b$, $\overline{k}_{\eta j}=\overline{k}_{\eta j+1}=\overline{k}_\eta$, $\overline{k}_{\theta j}=\overline{k}_{\theta j+1}=\overline{k}_\theta$, and $l_{j-1}=l_j=l_{j+1}=l$ in the dimensionless equations of motion for the $j$th car. Then, the simplified equations are

$$2(1+\chi\mu)l\frac{\mathrm{d}^2y_{cj}}{\mathrm{d}\tau^2}+\frac{2\mu l}{\pi}(C_Nu+c)\frac{\mathrm{d}y_{cj}}{\mathrm{d}\tau}+2\chi\mu lu\frac{\mathrm{d}\alpha_j}{\mathrm{d}\tau}-\overline{k}_\eta(y_{cj+1}-2y_{cj}+y_{cj-1})$$
$$+\overline{k}_\eta l(\alpha_{j+1}-\alpha_{j-1})-\frac{2\mu l}{\pi}\left\{\left(1-\frac{\varepsilon-1}{r_h}\right)C_T-C_N\right\}u^2\alpha_j+2\overline{k}_by_{cj}=0, \tag{1}$$

$$2l\left\{\frac{1}{4}+\frac{l^2}{3}(1+\chi\mu)\right\}\frac{\mathrm{d}^2\alpha_j}{\mathrm{d}\tau^2}-2\chi\mu lu\frac{\mathrm{d}y_{cj}}{\mathrm{d}\tau}+\frac{2\mu l^3}{3\pi}(C_Nu+c)\frac{\mathrm{d}\alpha_j}{\mathrm{d}\tau}+(-\overline{k}_\theta+\overline{k}_\eta l^2)(\alpha_{j+1}-2\alpha_j+\alpha_{j-1})$$
$$+\overline{k}_\eta l(y_{cj-1}-y_{cj+1})+(2\beta^2\overline{k}_bl^2+4\overline{k}_\eta l^2-2\chi\mu lu^2)\alpha_j=0. \tag{2}$$

Assuming travelling-wave solutions of the form

$$y_j=Y\,\mathrm{e}^{\mathrm{i}(\omega\tau-kL_j)}\quad\text{and}\quad\alpha_j=A_\alpha\,\mathrm{e}^{\mathrm{i}(\omega\tau-kL_j)}, \tag{3}$$

where $\omega$ is the dimensionless frequency, $\tau$ the dimensionless time, $k$ the dimensionless wavenumber, and

$$L_j=2\sum_{k=1}^{j-1}l_k+l_j \tag{4}$$

is the dimensionless length from the head of the train to the middle point of the $j$th cylindrical car, which is used in place of the continuous location $x$ [cf. Harrison and Nettleton (1997)]. Introducing the notation $B_\sigma=(2\mu l/\pi)\{[1-(\varepsilon-1)/r_h]C_T-C_N\}$, $B_\alpha=(2\mu l/\pi)(C_Nu+c)$, and $B_\beta=2\chi\mu lu$ the travelling-wave solution to Eq. (1) yields

$$\frac{A_\alpha}{Y}=\frac{2\omega^2(1+\chi\mu)l-\mathrm{i}\omega B_\alpha+2\overline{k}_\eta(\cos k-1)-2\overline{k}_b}{-2\mathrm{i}\overline{k}_\eta l\sin k+\mathrm{i}\omega B_\beta-B_\sigma u^2}. \tag{5}$$

In the same manner, for Eq. (2), letting $B_\chi=2\beta^2\overline{k}_bl^2+4\overline{k}_\eta l^2-2\chi\mu lu^2$, $B_J=2l\{\frac{1}{4}+\frac{1}{3}l^2(1+\chi\mu)\}$, and $B_\varepsilon=(2\mu l^3/3\pi)(C_Nu+c)$, we obtain

$$\frac{A_\alpha}{Y}=\frac{\mathrm{i}(\omega B_\beta-2\overline{k}_\eta l\sin k)}{-B_J\omega^2+\mathrm{i}B_\varepsilon\omega+2(-\overline{k}_\theta+\overline{k}_\eta l^2)(\cos k-1)+B_\chi}. \tag{6}$$

Combining Eqs. (5) and (6) and grouping terms in $\omega$, the following fourth-order polynomial is obtained:

$$2B_J(1+\chi\mu)l\omega^4 - \mathrm{i}\{B_JB_\alpha + 2B_\varepsilon(1+\chi\mu)l\}\omega^3 + [-B_\beta^2 - B_\varepsilon B_\alpha + 2B_J\{\overline{k}_\eta(\cos k - 1) - \overline{k}_b\} - 2(1+\chi\mu)l\{2(-\overline{k}_\theta + \overline{k}_\eta l^2)(\cos k - 1) + B_\chi\}]\omega^2 + [4B_\beta\overline{k}_\eta l \sin k + \mathrm{i}(-B_\beta B_\sigma u^2 - 2B_\varepsilon\{\overline{k}_\eta(\cos k - 1) - \overline{k}_b\} + B_\alpha\{2(-\overline{k}_\theta + \overline{k}_\eta l^2)(\cos k - 1) + B_\chi\})]\omega + [-4(\overline{k}_\eta l \sin k)^2 - 2\{2(-\overline{k}_\theta + \overline{k}_\eta l^2)(\cos k - 1) + B_\chi\}\{\overline{k}_\eta(\cos k - 1) - \overline{k}_b\} + \mathrm{i}(2\overline{k}_\eta l B_\sigma u^2 \sin k)] = 0. \quad (7)$$

Eq. (7) will be solved numerically for $\omega$ for varying values of $k$.

If, instead of Eqs. (3), solutions of the following form are assumed:

$$y_j = Y\,\mathrm{e}^{\mathrm{i}\omega\tau}\,\mathrm{e}^{-kL_j} \quad \text{and} \quad \alpha_j = A_\alpha\,\mathrm{e}^{\mathrm{i}\omega\tau}\,\mathrm{e}^{-kL_j}, \quad (8)$$

for Eqs. (1) and (2), dispersion relations are obtained for decaying waves along the length of the train, with the amplitude of the waves decaying exponentially as they propagate. For decaying waves, a solution similar to Eq. (7) is obtained, except that the cosine and sine terms are replaced by hyperbolic functions.

### 2.2. Free wave propagation in vacuum

The formulation of the dispersion relation of an infinite-length train in air in a tunnel has been derived and is given by Eq. (7). In this section, based on this formulation, the dynamics of the train in vacuum will be studied and compared to previous work by Manabe (2002), in which the equations of motion were transformed into simultaneous homogeneous difference equations and solved via an eigenvalue analysis. The values for the system parameters of the infinite-length train in a tunnel are given in Table 1. For the sake of clarity, all mechanical damping terms are set to zero. A fixed position of the supporting springs is employed by considering typical arrangements of high-speed trains: bogie cars or articulated ones, as illustrated in Fig. 1. We use $\beta = 0$ to represent supports at the centre of the car and $\beta = 1$ for supports at the end of a car; $\beta = 0.72$ is used for bogie cars and $\beta = 1$ for articulated ones (Fujimoto, 1999).

The infinite-length train has two vibrational mode shapes as shown in Fig. 2. Each car, which is the component substructure of the train model, has two degrees of freedom in the lateral translational and yawing directions. Similarly, because the number of mode shapes of a periodic structure generally corresponds to that of the degrees of freedom of each component (Brillouin, 1946), the infinite-length train may be considered to have two modes. Here, we call the translational motion Mode 1, and the rotational one Mode 2.

Next, we illustrate the results obtained in terms of both the dimensional and the dimensionless dispersion relations; the dimensional relation gives a better image of the motion of actual trains. The particular case of $\beta = 1$ and $\rho_f = 0$, which represents articulated cars in a vacuum, is considered. Figs. 3 and 4 show the frequency–wavelength (wavenumber) relationship, i.e., the dispersion characteristics, as well as the phase and group velocities $c_{ph}$ and $c_{gp}$, which are defined as follows:

$$c_{ph} = \frac{\omega}{k} \quad \text{and} \quad c_{gp} = \frac{\mathrm{d}\omega}{\mathrm{d}k}. \quad (9)$$

The velocities $c_{ph}$ and $c_{gp}$ are plotted against wavelength $\lambda$ (m) in Fig. 3(b) and against frequency $f$ (Hz) in Fig. 4. In addition, the amplitude ratio $l\alpha/y$, where $y$ and $l\alpha$ are the displacements at the ends of each car for translational and rotational motions, respectively, is illustrated in Fig. 4(a).

Table 1
System parameters of the infinite-length train employed for the wave propagation analysis

| | |
|---|---|
| $N = \infty$ | $2l_j(= l_{\mathrm{car}}) = 14.12$ (25 m) |
| $L_A = \infty$ | $a = 1.77$ m |
| $R^*/a = 2.24$ (in a tunnel) or $\infty$ (in vacuum) | $A/A_d = 0.2$ (in a tunnel) or $\infty$ (in vacuum) |
| $\rho_f = 1.23\,\mathrm{kg/m^3}$ (in air) or 0 (in vacuum) | $\rho_{\mathrm{car}} = 151.6\,\mathrm{kg/m^3}$ |
| $\beta = 0.72$ or 1.0 | $A'/A = 1.0$ |
| $C_T = 0.01288$ | $C_N = C_T$ or $C_T/1.4$ |
| $C_D = 0$ | $C_b = 0.157$ |
| $f_n = 1.0$ | $f_t = 0.8$ |
| $k_f = k_b = 3.53 \times 10^5\,\mathrm{N/m}$ | $k_\alpha = 0\,\mathrm{N\,m/rad}$ |
| $k_\eta = 9.8 \times 10^3\,\mathrm{N/m}$ | $k_0 = 1.0 \times 10^4\,\mathrm{N/m}$ |

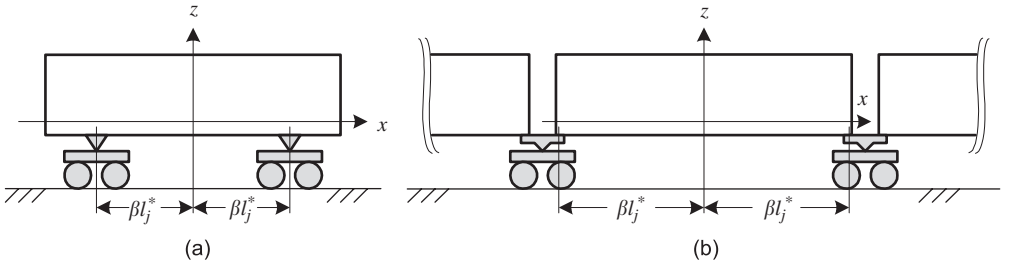


Fig. 1. Typical side view geometry of trains: (a) bogie car and (b) articulated car.

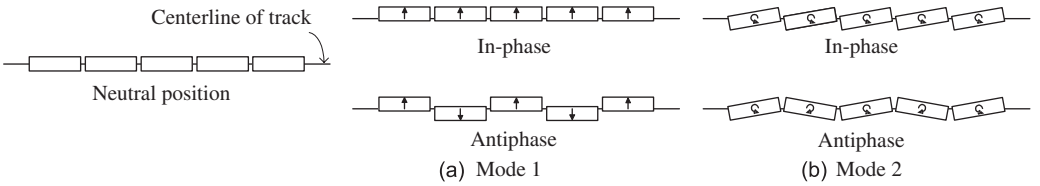


Fig. 2. Mode shapes of wave propagation in an infinite-length train (top view); only five cars are shown for the sake of clarity.

As shown in Figs. 3(a) and 4(a), there are two "propagation bands": one in the frequency range 0.71–0.73 Hz corresponding to Mode 1, and the second in the frequency range 1.26–1.73 Hz corresponding to Mode 2. Consequently, waves can propagate freely (i.e., unattenuated) in the train, forward or backwards, only within these two frequency bands. These bands correspond to the two mode shapes shown in Fig. 2. The reason that the lower frequency band (0.71–0.73 Hz) corresponds to Mode 1 and the higher one (1.26–1.73 Hz) to Mode 2 can be understood from the amplitude ratio $l\alpha/y$ shown in Fig. 4(a). As can be seen in the figure, the amplitude ratio of the lower frequency band (0.71–0.73 Hz) is quite small ($\leqslant 10^{-2}$), or equivalently $y \gg l\alpha$, indicating that the displacement of the translational motion is dominant in the lower frequency band. Accordingly, the lower frequency band corresponds to Mode 1 as shown in Fig. 2. On the other hand, the amplitude ratio of the higher frequency band (1.26–1.73 Hz) is quite large ($\geqslant 10^2$), or equivalently $y \ll l\alpha$, indicating that the displacement of the cars is mainly one of yawing in the higher frequency band. Therefore, the higher frequency band corresponds to Mode 2.

Fig. 4(a) shows that the phase and group velocities of the present solutions agree very well with those of Manabe's (2002), which confirms the formulation of the dispersion relation.

As shown in Fig. 3, frequency peaks and valleys occur at $\lambda_1, \lambda_2, \ldots, \lambda_n$. The first peak at $\lambda_1$ corresponds to the minimum wavelength of the train, which is equal to the length of two cars, $2L_{\text{car}} = 50$ m. In this case, adjacent cars oscillate in opposing directions, which corresponds to the "antiphase" pattern of Modes 1 and 2, as shown in Fig. 2. The other peaks, $\lambda_2, \lambda_3, \ldots, \lambda_n$, correspond to aliasing waves ($\lambda_n = 50/n; n = 2, 3, \ldots$) below the minimum wavelength. On the other hand, the maximum wavelength of the train ($\lambda \geqslant 400\,\text{m} = 16L_{\text{car}}$) corresponds to the "in-phase" patterns of Modes 1 and 2 in Fig. 2, where all the cars oscillate in the same direction.

From Fig. 4(a) it is seen that the phase velocity of Mode 1 decreases from $1.0 \times 10^3$ m/s at 0.71 Hz to 37 m/s at 0.73 Hz, while that of Mode 2 from $1.0 \times 10^3$ m/s at 1.26 Hz to 87 m/s at 1.73 Hz. From Fig. 4(a) it is shown that the group velocities at the extremities of the upper and lower frequency bands of Modes 1 and 2 become nearly zero, while in the middle of each band the group velocities of Modes 1 and 2 are approximately 1.4 and 36 m/s, respectively. Note that the frequencies at the extremities of the lower frequency bands of Modes 1 and 2 correspond to the "in-phase" mode, and those of the upper one to the "antiphase" mode, respectively, as shown in Fig. 2. The phase velocities become almost infinity at the extremities of the lower frequency bands of Modes 1 and 2 because all cars in the train vibrate in phase. The group velocities, which correspond to the propagation of energy, at the extremities of the upper and lower frequency bands of Modes 1 and 2 become nearly zero because the vibrations of the cars correspond to standing waves. On the other hand, the group velocities in the middle of each band have peaks but they are always lower than the phase velocities.

As mentioned in the foregoing section, it is known that, when the velocity of a harmonic travelling aerodynamic force approaches the minimum phase velocity along a periodic structure, there may be amplification of the disturbances, leading to the possibility of structural damage (Mead, 1971; Manabe, 2002). Typical running velocities of high-speed trains are in the range 50–90 m/s, which are of the same order as the phase and group velocities shown in Fig. 4(a). Running trains are subject to external perturbations from the surroundings; for example, from irregularities of the rails,

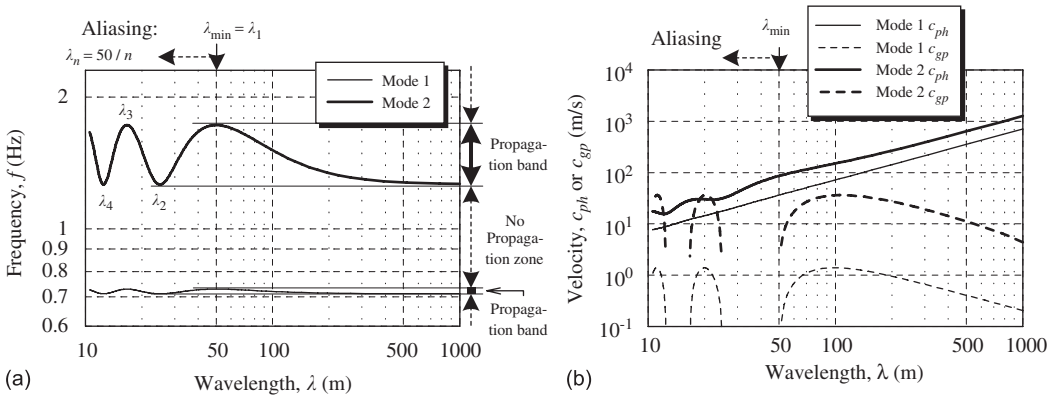


Fig. 3. (a) The dimensional dispersion relation and (b) the phase and group velocities $c_{ph}$ and $c_{gp}$ of the infinite-length train in vacuum.

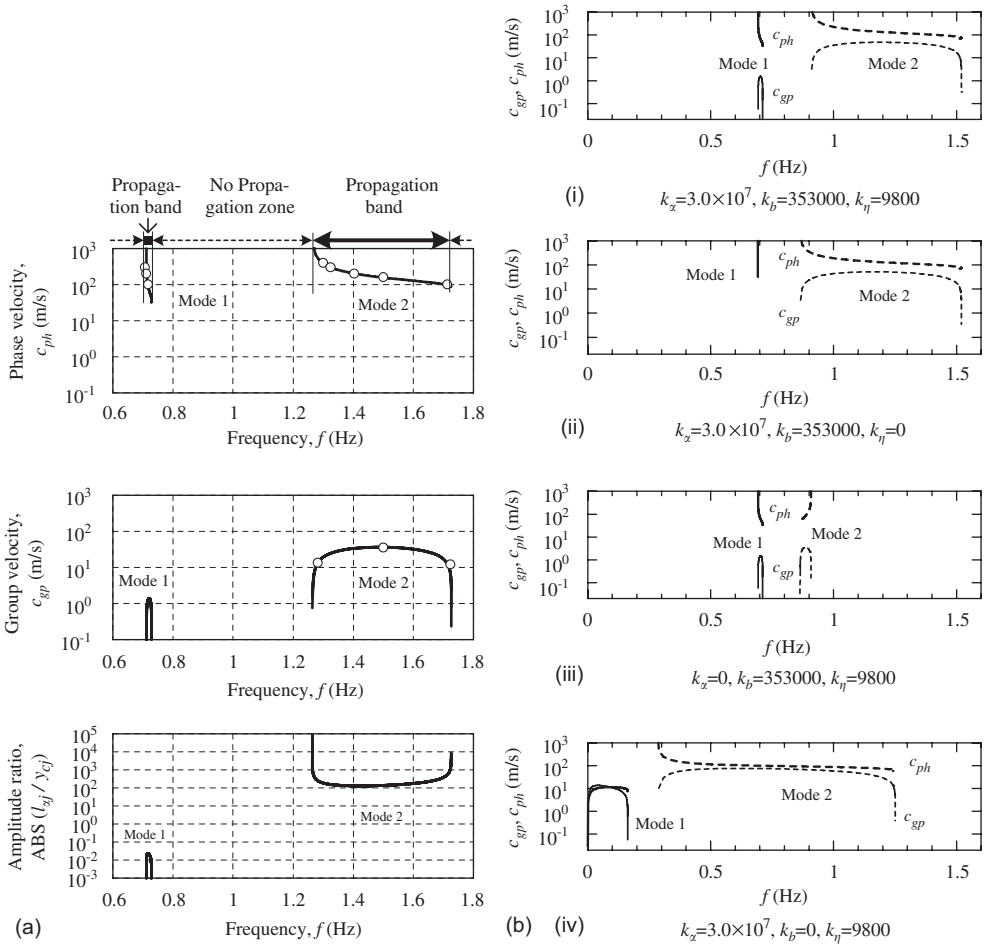


Fig. 4. (a) The phase and group velocities $c_{ph}$ and $c_{gp}$, and amplitude ratio $l\alpha_j / y_{cj}$ at the ends of each car for an infinite-length train with all springs ($k_\theta$, $k_b$, $k_\eta$) attached. $\rho_f = 0$, $\beta = 1.0$, no aerodynamic forces, and no mechanical damping: —, present solution; ◯, Manabe's (2002) solution. (b) Effect of spring stiffnesses $k_\alpha$, $k_b$, and $k_\eta$ on the phase and group velocities $c_{ph}$ and $c_{gp}$. ($\rho_f = 0$, $\beta = 0.72$, no aerodynamic forces and no mechanical damping.)

overhead line equipment, and air disturbances. In other words, in the train coordinate system, these perturbations travel along the train. Hence, these perturbations may have an influence on the dynamics of the train. Later, in Section 3, the response of the system will be studied when the velocity of a moving force along the train approaches the minimum phase velocity for a travelling wave in the train.

### 2.3. The effect of translational, rotational, and supporting springs on wave propagation in vacuum

In the previous section, the formulation of the dispersion relation was verified by comparing the results obtained with previous work by Manabe (2002). In this section the effects of the translational (or shearing) and rotational (or bending) springs between cars, and of the position of supporting springs ($\beta = 0.72$ and 1.0) on wave propagation in vacuum ($\rho_f = 0$) are examined.

Fig. 4(b) illustrates the effect of the spring stiffness on wave propagation. The top part of Fig. 4(b), for the case where all the springs have non-zero values, shows that the frequency band of Mode 2 (the rotational mode from 0.91 to 1.52 Hz) is wider than that of Mode 1 (the translational mode from 0.69 to 0.71 Hz), and the frequency band of Mode 2 is higher than that of Mode 1. This is also the case for the other results shown in Fig. 4(b) as well. The effect of the position of the supporting springs can be seen by comparing the results of Fig. 4(a) ($\beta = 1.0$) with those of Fig. 4(b) ($\beta = 0.72$). Recall that $\beta = 0.72$ represents bogie cars and $\beta = 1$ articulated ones, as illustrated in Fig. 1. Figs. 4(a) and (b) show that, as the supporting position changes from $\beta = 1$ to 0.72, the band of Mode 1 moves from the range 0.71–0.73 to 0.69–0.71 Hz, and that of Mode 2 from 1.26–1.73 to 0.91–1.52 Hz. Moreover, the range of frequencies in the bands is reduced to some extent. Thus, it is demonstrated that the position of the supporting springs has some effect on wave propagation in the infinite-length train.

The second part of Fig. 4(b), corresponding to the case with no translational springs, $k_\eta = 0$, indicates that no propagation band exists for the translational mode (Mode 1). The third part of Fig. 4(b), corresponding to no rotational springs, $k_\alpha = 0$, shows that the range of Mode 2 is significantly narrower than for the other cases. Hence, the rotational springs $k_\alpha$ have a considerable effect on the wave propagation for Mode 2. It should be noted that, even without rotational springs, a narrow propagation band of the rotational mode (Mode 2) exists. The bottom part of Fig. 4(b) shows the case with no supporting springs, $k_b = 0$, and the bands of both Modes 1 and 2 are wider than in the other cases. Note that the lower bounding frequency of Mode 1 becomes zero when $k_b = 0$.

### 2.4. Dimensionless dispersion relation

In the foregoing sections, the dimensional dispersion relations have been used to examine wave propagation in an infinite-length train. Hereafter, dimensionless dispersion relations will be used instead. The dimensionless equivalent of the results presented in Fig. 3 are shown in Fig. 5 and they give additional insight. The results in terms of dimensional and dimensionless dispersion relations are, of course, physically the same. However, for the results of Fig. 3 (dimensional) the wavelength $\lambda$ is used in the abscissa, whereas in Figs. 5 and 6 the dimensionless wavenumber $k$ is used instead. It is physically easier to appreciate a positive or negative $k$ for forward or backward travelling waves, and less easy to consider a negative wavelength. The dimensional results in Fig. 3(a) correspond to the dimensionless ones of the right half of Fig. 5(a).

As shown in Fig. 5(a), at the upper bounding frequencies of Mode 1 ($\omega \simeq 2.44$) and Mode 2 ($\omega \simeq 5.8$), the dimensionless wavenumber $k$ reaches the values of $\pm\pi$, where each car has maximum phase difference to the adjacent cars. This corresponds to the "antiphase" patterns in Fig. 2. In the same manner, when the dimensionless wavenumber is zero at the lower bounding frequencies of Mode 1 ($\omega \simeq 2.38$) and Mode 2 ($\omega \simeq 4.2$), the cars have zero phase difference with adjacent cars.

Note that the dispersion relations are symmetric with respect to $k = 0$, and thus the phase and group velocities $c_{ph}$ and $c_{gp}$ are also symmetric with respect to the origin ($c_{ph}$ or $c_{gp}, \omega$) $= (0, 0)$, as seen in Fig. 5(b). In this case, positive and negative waves exist travelling at the same speed. In other words, a standing wave may exist if a finite-length train is considered.

### 2.5. The effect of aerodynamic force on wave propagation

Wave propagation for the train in vacuum ($\rho_f = 0$) was examined in the foregoing sections. In this section, aerodynamic effects on wave propagation are taken into account for infinite-length trains of bogie cars ($\beta = 0.72$) and the articulated system ($\beta = 1.0$), cf. Fig. 1. Then, the effect of the Coriolis terms and the other fluid damping terms on the dispersion relation is examined.

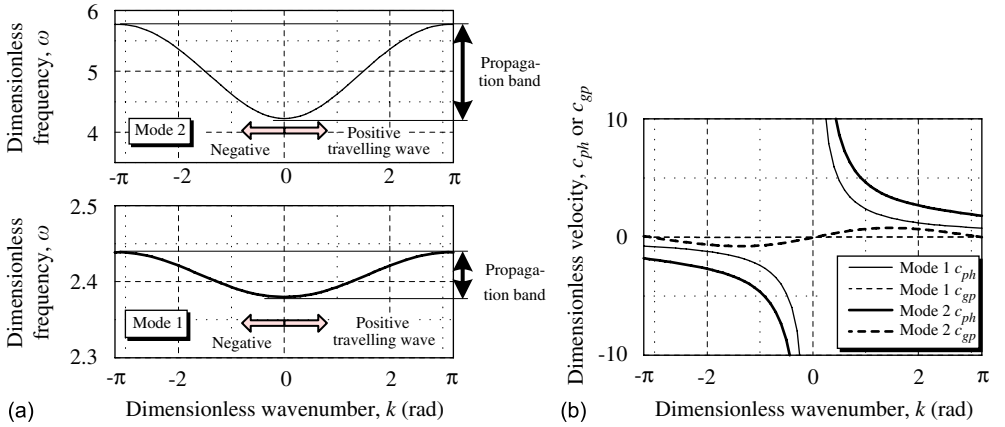


Fig. 5. The dimensionless dispersion relation and the phase and group velocities $c_{ph}$ and $c_{gp}$ of an infinite-length train in vacuum.

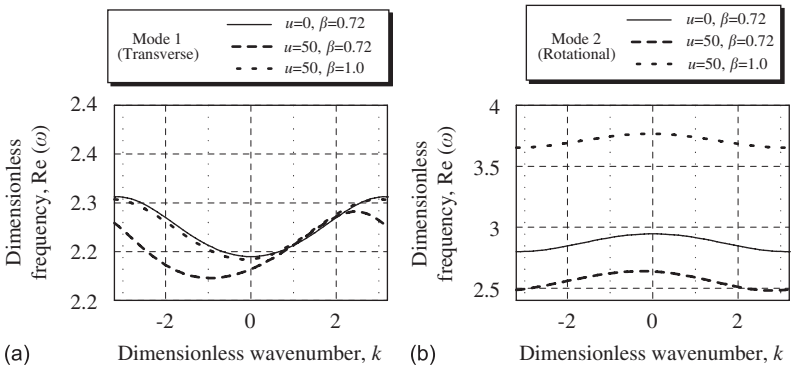


Fig. 6. The dimensionless dispersion relations for the infinite-length trains of bogie cars ($\beta = 0.72$) and articulated ones ($\beta = 1.0$) with $u = 0$ and 50; $C_N/C_T = 1.0$, $k_\alpha = 0$, $k_b = 353\,000$, $k_\eta = 9800$, no mechanical damping: (a) Mode 1, (b) Mode 2.

Fig. 6 shows the dimensionless dispersion relations for the infinite-length trains of bogie cars ($\beta = 0.72$) and the articulated system ($\beta = 1.0$) with $u = 0$ and 50. When the train is stationary ($u = 0$), the dispersion relations of Modes 1 and 2 are symmetric with respect to $k = 0$. In this case, the forward and backward travelling waves have the same frequencies, and thus standing waves may exist along the train, as explained in connection with Fig. 5. (Note that, since similar symmetric results are obtained for the case of $\beta = 1.0$, they are not given in Fig. 6.) When the train is moving at a velocity of $u = 50$ ($U = 166\,\text{m/s} \simeq 598\,\text{km/h}$),[1] for $\beta = 0.72$ both curves for Modes 1 and 2 shift to lower dimensionless frequencies (downwards) and also to lower dimensionless wavenumber (to the left). In addition, the shift to lower dimensionless wavenumber is considerably larger for Mode 1 than for Mode 2. For $\beta = 1.0$ with $u = 50$, the results are similar, but the shifts are much smaller than for $\beta = 0.72$; excepting that the curve of Mode 2 shifts to a higher frequency.

Next, the effect of these shifts on the dispersion relations due to the aerodynamic force is investigated. It has been shown (Chen and Rosenberg, 1971; Païdoussis, 1998) that the presence of the Coriolis term in the equation of motion renders the phase velocity different for the forward and the backward travelling waves in a supported pipe conveying fluid. Thus, the effect of the Coriolis terms, as well as the fluid damping terms (including the Coriolis terms), on the aforementioned shifts is examined. This is done by comparing dispersion relations obtained from the equations of motion with and without these terms. The Coriolis terms in Eqs. (1) and (2) are $2\chi\mu lu(\mathrm{d}\alpha_j/\mathrm{d}\tau)$ and

[1]Note that even though the relative velocity of air, $U = 166\,\text{m/s}$ ($\simeq 598\,\text{km/h}$) may appear to be impractical, the Magnetic Levitation (MAGLEV) train in Japan is being tested at speeds in the 500 km/h range, and its top speed may be increased even more in the future (Sawada, 2000). On 2nd December 2003, the three-car MAGLEV train attained a maximum speed of 581 km/h in a manned vehicle run.

$(2\mu l^3 C_N u/3\pi)(\mathrm{d}\alpha_j/\mathrm{d}\tau)$, respectively. The fluid damping terms, which are the first-order derivatives of $y_{cj}$ and $\alpha_j$ with respect to time, in Eqs. (1) and (2) are $(2\mu l/\pi)(C_N u + c)(\mathrm{d}y_{cj}/\mathrm{d}\tau) + 2\chi\mu l u(\mathrm{d}\alpha_j/\mathrm{d}\tau)$ and $-2\chi\mu u l(\mathrm{d}y_{cj}/\mathrm{d}\tau) + (2\mu l^3/3\pi)(C_N u + c)(\mathrm{d}\alpha_j/\mathrm{d}\tau)$, respectively. The dispersion results obtained with and without these terms are shown in Fig. 7. When only the Coriolis forces are deleted, the shifts are much smaller than for the case which includes the fluid damping terms. On the other hand, when the fluid damping terms including the Coriolis ones are deleted, the curves (solid lines) become symmetric with respect to $k = 0$. Therefore, the fluid damping terms, including the Coriolis terms, are the main cause of these shifts, and that these terms render classical normal modes impossible.

To examine the effect of viscous frictional drag on the system, a calculation with $C_N/C_T = 1.4$ was conducted, but exactly the same results as for $C_N/C_T = 1.0$ (shown in Fig. 7) were obtained (hence, no figures are shown). Therefore, it can be concluded that the ratio between $C_T$ and $C_N$ has very little effect on the dispersion relation, even though it has a considerable effect on the stability of the train, as shown in Part 1 (Sakuma et al., 2008). This is because the term accounting for $C_T$ and $C_N$, $-(2\mu l/\pi)\{[1-(\varepsilon-1)/r_h]C_T - C_N\}u^2\alpha_j$, is not involved in the fluid damping terms.

Finally, the relationship between the dimensionless frequency $\mathrm{Re}(\omega)$ and dimensionless flow velocity $u$ for forward travelling waves [upper branch where $\mathrm{Re}(\omega)>0$] and backward travelling ones [lower branch where $\mathrm{Re}(\omega)<0$] is illustrated in Fig. 8 for dimensionless wavenumbers $k = \pi$ and $k = 0.1\pi$. Note that the present analysis assumes incompressible flow over slender bodies, and thus the values of $\omega$ where $u>90$ or $U = 300\,\mathrm{m/s}$ are shown just for reference. As seen in Fig. 8, irrespective of whether $k = \pi$ or $k = 0.1\pi$, both loci are almost symmetric with respect to the $\mathrm{Re}(\omega) = 0$ axis, even though the two absolute values of $\omega$ for the upper and lower branches are not exactly equal at the same flow velocity. Also, the loci for $k = \pi$ coalesce at $u \simeq 104$, and those for $k = 0.1\pi$ at $u \simeq 109$, practically on the $u$-axis. In general, at the point of crossing the $u$-axis, the negative $\mathrm{Re}(\omega)$ becomes zero, and thus there is no longer a backward travelling wave, which physically corresponds to a divergence. On the other hand, the point of coalescence of

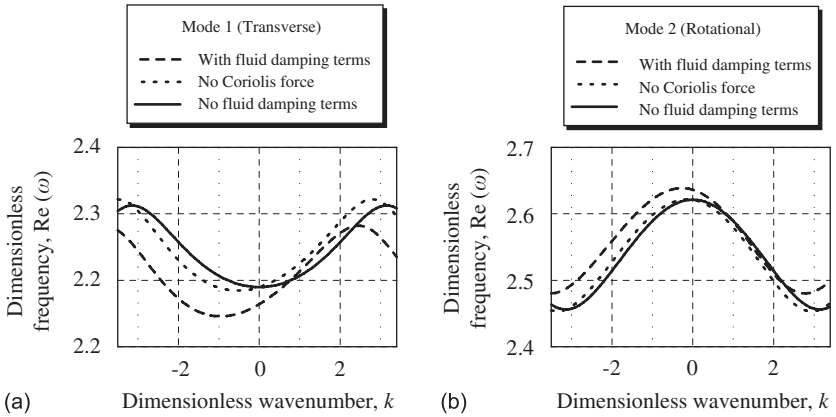


Fig. 7. Effect of fluid damping terms on wave propagation for an infinite-length train; $C_N/C_T = 1.0$, $\beta = 0.72$, $k_\alpha = 0$, $k_b = 353\,000$, $k_\eta = 9800$, no mechanical damping: (a) Mode 1, (b) Mode 2.

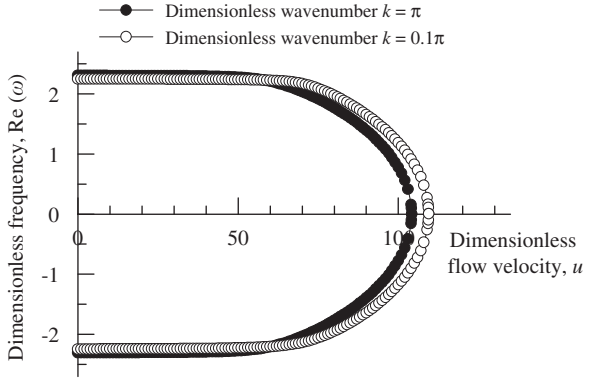


Fig. 8. The relationship between the dimensionless frequency $\mathrm{Re}(\omega)$ and dimensionless flow velocity $u$ for dimensionless wavenumbers $k = \pi$ and $k = 0.1\pi$; $C_N/C_T = 1.0$, $\beta = 0.72$, $k_\alpha = 0$, $k_b = 353\,000$, $k_\eta = 9800$, no mechanical damping.

the two solution branches corresponds to where $\omega$ becomes complex, and is the critical value for flutter. It should be kept in mind that, in the range of the flow velocities we analyze ($u \leqslant 90$), neither divergence nor flutter can be observed in the present system for the infinite-length train.

## 3. Transient and steady-state response of the LTB train to a travelling aerodynamic force along the train

In this section, the response of a finite-length train to a travelling sinusoidal aerodynamic force is studied; this simulates the features obtained during running experiments on real trains. In addition, the response of the system is examined when the velocity of the force approaches the minimum phase velocity of the travelling wave obtained in Section 2.

First, based on previous work for a *single* car by Suzuki (1999), the lateral force and yawing moment, $Q_{y_{cj}}(t)$ and $Q_{\alpha_j}(t)$, acting on *cars* in the *finite-length LTB train* are obtained. Second, some features of the lateral force and yawing moment will be illustrated. In particular, the phase difference between two adjacent cars will be examined analytically. Third, the lateral force and yawing moment will be combined with the equations of motion derived in Part 1 (Sakuma et al., 2008). Fourth, the transient response of the train and its mode shapes when the train is subjected to sinusoidal aerodynamic forces with four different wavelengths (17.5, 25, 30, and 33.3 m) will be obtained by using Runge–Kutta numerical integration of the equations of motion. The effects of the wavelength of the sinusoidal aerodynamic force on the mode shapes of the finite-length train are then clarified. The steady-state mode shapes are compared to those of previous work obtained from running experiments. Finally, the response of a train to the force moving at the minimum phase velocity of the travelling wave in the train, obtained in Section 2, is examined.

### 3.1. Travelling aerodynamic force along the train

#### 3.1.1. Assumptions

The following features obtained from running experiments on real trains (Sakuma et al., 1998; Suzuki, 2001) are assumed:

(i) large-scale coherent structures exist, which move downstream in the space between the side of the train and the tunnel wall at a speed equivalent to about 80% of the train speed;
(ii) the amplitude of the aerodynamic force, $F_E^*$, acting on the cars is directly proportional to the square of the air velocity;
(iii) a dimensionless coefficient, $C_E$, and frequency, St, of the force can be defined from the foregoing as $C_E \sim 0.06$ and $\mathrm{St} \sim 0.1$, respectively, where $\mathrm{St} = 2af_E/U$, $\omega_E = 2\pi f_E$, and $C_E = F_E^*/(\frac{1}{2}\rho a U^2)$.

In addition, the wavelength of the travelling sinusoidal force is assumed to be constant along the entire length of the train.

#### 3.1.2. Derivation of the generalized force

Fig. 9 shows a schematic of the sinusoidal aerodynamic force travelling along five adjacent cars, from the head toward the tail of the train. The travelling aerodynamic force, per unit length of the train, is assumed to be a sinusoidal wave, and is given by

$$F_{EX}(x^*, t, U) = F_E^*(U)\cos(k^* x^* - \omega_E^* t) = F_E^*(U)\cos(k^*(L_j^* + \xi^*) - \omega_E^* t), \tag{10}$$

where

$$L_j^* = 2\sum_{k=1}^{j-1} l_k^* + l_j^* \tag{11}$$

is the length from the head of the train to the middle point of the $j$th cylindrical car, $k^* = 2\pi/\lambda_E^*$ is the wavenumber of the aerodynamic force, $f_E^*$ the frequency, $\omega_E^* = 2\pi f_E^*$ the circular frequency, $V_E = f_E^*\lambda_E^* = \omega_E^*/k^*$ the travelling speed of the aerodynamic force, and $\xi^*$ the local coordinate on the $j$th car which is related to the $x^*$ coordinate by

$$x^* = 2\sum_{k=1}^{j-1} l_k^* + l_j^* + \xi^* = L_j^* + \xi^*. \tag{12}$$

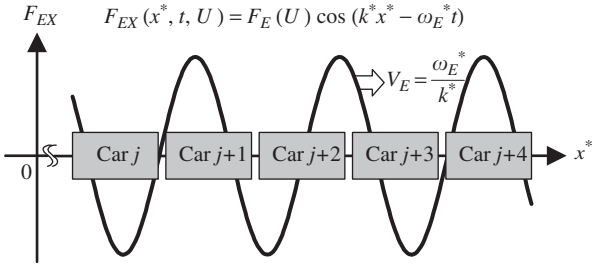


Fig. 9. Schematic of the sinusoidal aerodynamic force travelling from the head toward the tail of the five adjacent cars in the train.

Variables with an asterisk are dimensional values. The virtual work done by the aerodynamic force associated with virtual displacements $\delta(y_{cj}^* + \xi^* \alpha_j)$ is given by

$$\delta W_j = \int_{-l_j^*}^{l_j^*} F_{EX}\delta(y_{cj}^* + \xi^*\alpha_j)\,\mathrm{d}\xi. \tag{13}$$

Hence, the generalized forces $\hat{Q}_{y_{cj}}$ (lateral force) and $\hat{Q}_{\alpha_j}$ (yawing moment) on the $j$th cylindrical car are

$$\begin{aligned}\hat{Q}_{y_{cj}} &= \left.\frac{\delta W_j}{\delta y_{cj}^*}\right|_{\delta\alpha_j=0} = \frac{F_E^*}{k^*}[\sin\{k^*(L_j^* + l_j^*) - \omega_E^* t\} - \sin\{k^*(L_j^* - l_j^*) - \omega_E^* t\}],\\ &= \frac{\lambda_E^* F_E^*}{\pi}\sin\left(\frac{2\pi l_j^*}{\lambda_E^*}\right)\cos\left(\frac{2\pi L_j^*}{\lambda_E^*} - \omega_E^* t\right),\end{aligned} \tag{14}$$

$$\begin{aligned}\hat{Q}_{\alpha_j} &= \left.\frac{\delta W_j}{\delta \alpha_j}\right|_{\delta y_{cj}^*=0} = \frac{F_E^* l_j^*}{k^*}[\sin\{k^*(L_j^* + l_j^*) - \omega_E^* t\} + \sin\{k^*(L_j^* - l_j^*) - \omega_E^* t\}]\\ &\quad + \frac{F_E^*}{k^{*2}}[\cos\{k^*(L_j^* + l_j^*) - \omega_E^* t\} - \cos\{k^*(L_j^* - l_j^*) - \omega_E^* t\}]\\ &= \frac{\lambda_E^* F_E^*}{\pi}\left\{l_j^*\cos\left(\frac{2\pi}{\lambda_E^*} l_j^*\right) - \frac{\lambda_E^*}{2\pi}\sin\left(\frac{2\pi}{\lambda_E^*} l_j^*\right)\right\}\sin\left(\frac{2\pi}{\lambda_E^*} L_j^* - \omega_E^* t\right).\end{aligned} \tag{15}$$

Letting $F_E^* = \frac{1}{2} C_E \rho a U^2$, where $C_E$ is the coefficient of the travelling aerodynamic force, introducing the dimensionless quantities

$$l = l^*/a, \quad \lambda_E = \lambda_E^*/a, \quad \tau = t\sqrt{\frac{k_0}{m_0 a}}, \quad u = U\sqrt{\frac{m_0}{k_0 a}}, \quad \omega_E = \omega_E^*\sqrt{\frac{m_0 a}{k_0}}, \quad \mu = \frac{M_0}{m_0},$$

where $k_0$ is the reference coefficient for translational spring between the cylinders and the duct, $m_0$ the mass of cylinder per unit length, and $M_0$ the virtual mass of the fluid per unit length of the cylinder, and noting that

$$\lambda_E^* F_E^* = a\lambda_E \frac{1}{2} C_E \rho a U^2 = \frac{1}{2} a\lambda_E C_E \left(\frac{M_0}{\pi a^2}\right) a\left(\frac{k_0 a}{m_0} u^2\right) = \frac{\mu\lambda_E C_E}{2\pi}(k_0 a)u^2,$$

the generalized force may be written as

$$\hat{Q}_{y_{cj}} = \frac{\mu\lambda_E C_E}{2\pi^2}(k_0 a)u^2 \sin\left(\frac{2\pi l_j}{\lambda_E}\right)\cos\left(\frac{2\pi L_j}{\lambda_E} - \omega_E \tau\right).$$

To be consistent with the equations given in Part 1, we obtain the following for the *dimensionless* generalized aerodynamic force for the $j$th car:

$$Q_{y_{cj}} = \frac{\hat{Q}_{y_{cj}}}{a k_0} = \frac{\mu\lambda_E C_E u^2}{2\pi^2}\sin\left(\frac{2\pi l_j}{\lambda_E}\right)\cos\left(\frac{2\pi}{\lambda_E} L_j - \omega_E \tau\right). \tag{16}$$

Then, its amplitude, $\overline{Q}_{y_{cj}}$, is

$$\overline{Q}_{y_{cj}} = \frac{\mu\lambda_E C_E u^2}{2\pi^2}\sin\left(\frac{2\pi l_j}{\lambda_E}\right). \tag{17}$$

In the same manner, for the yawing moment we have

$$\hat{Q}_{\alpha_j} = \frac{\mu\lambda_E C_E}{2\pi^2}(k_0 a^2)u^2\left\{l_j\cos\left(\frac{2\pi}{\lambda_E}l_j\right) - \frac{\lambda_E}{2\pi}\sin\left(\frac{2\pi}{\lambda_E}l_j\right)\right\}\sin\left(\frac{2\pi}{\lambda_E}L_j - \omega_E\tau\right);$$

and hence the dimensionless yawing moment $Q_{\alpha_j} = \hat{Q}_{\alpha_j}/ak_0^2$ is given by

$$Q_{\alpha_j} = \frac{\mu\lambda_E C_E u^2}{2\pi^2}\left\{l_j\cos\left(\frac{2\pi}{\lambda_E}l_j\right) - \frac{\lambda_E}{2\pi}\sin\left(\frac{2\pi}{\lambda_E}l_j\right)\right\}\sin\left(\frac{2\pi}{\lambda_E}L_j - \omega_E\tau\right) \tag{18}$$

and its amplitude, $\overline{Q}_{\alpha_j}$, is

$$\overline{Q}_{\alpha_j} = \frac{\mu\lambda_E C_E u^2}{2\pi^2}\left\{l_j\cos\left(\frac{2\pi}{\lambda_E}l_j\right) - \frac{\lambda_E}{2\pi}\sin\left(\frac{2\pi}{\lambda_E}l_j\right)\right\}. \tag{19}$$

*3.1.3. Features of the force*

The generalized forces for the travelling aerodynamic force along the train were derived in Section 3.1.2. Here, some features of $Q_{y_{cj}}(t)$ and $Q_{\alpha_j}(t)$ are examined.

The amplitudes of both forces, $Q_{y_{cj}}$ and $Q_{\alpha_j}$, are a function of the wavelength $\lambda_E$, as seen in Eqs. (17) and (19) and illustrated in Fig. 10. The vertical axes are arbitrarily scaled with respect to the absolute values for a wavelength of 30 m. Increasing the wavelength from zero, the envelopes of the absolute amplitudes of both forces increase; this is because the coefficient $\mu\lambda_E C_E u^2/(2\pi^2)$ in Eqs. (17) and (19) is directly proportional to wavelength. On the other hand, both forces periodically become zero because of their dependence on the trigonometric sine and cosine functions. As seen in Eq. (17), $\overline{Q}_{y_{cj}}$ is proportional to $\sin(2\pi l_j^*/\lambda_E^*)$ and becomes zero when $2\pi l_j^*/\lambda_E^* = n\pi$ or $\lambda_E^* = 2l_j^*/n = 25/n$, where $n$ is a positive integer and $2l_j^* = l_{\text{car}} = 25$ m as given in Table 2. Hence, the lateral force, $Q_{y_{cj}}(t)$, becomes zero when $\lambda_E^* = 25/n = 25.0, 12.5, 8.33, \ldots$ for $n = 1, 2, 3, \ldots$, respectively, as seen in Fig. 10; thus, for these wavelengths no lateral force acts on the cars. Searching for the wavelengths at which the yawing moment becomes zero is more complicated than for the lateral force; this is because $Q_{\alpha_j}(t)$ is proportional to $\{l_j\cos(2\pi l_j/\lambda_E) - (\lambda_E/2\pi)\sin(2\pi l_j/\lambda_E)\}$. As seen in Fig. 10 for example, the yawing moment becomes zero at a wavelength of 17.5 m. Therefore, it is expected that the response of the cars to a sinusoidal aerodynamic force with certain wavelengths, such as 17.5 and 25 m, will be purely lateral translational or rotational motion. This will be demonstrated in Section 3.3. As shown in Eqs. (16) and (18), $Q_{y_{cj}}$ is proportional to $\cos(2\pi L_j/\lambda_E - \omega_E\tau)$, while $Q_{\alpha_j}$ to $\sin(2\pi L_j/\lambda_E - \omega_E\tau)$. Because the cosine function leads the sine by 90°, the lateral force $Q_{y_{cj}}$ leads the yawing moment $Q_{\alpha_j}$ by 90°. Hence, the cars are expected to move first in the lateral direction and then in the rotational one. The features of the forces obtained here are in good agreement with those of previous results for a single car by Suzuki (1999).

In the foregoing, the phase relationship between $Q_{y_{cj}}(t)$ and $Q_{\alpha_j}(t)$ for a *single* car was given. Next, the phase relationship between *two adjacent cars*, Car $j+1$ and Car $j$, in the train is examined. Since the length of all cars is $2l$, using Eq. (11) we have

$$L_{j+1} = L_j + 2l. \tag{20}$$

Substituting Eq. (20) into Eq. (16) with $L_{j+1}$ replacing $L_j$, we obtain

$$\cos\left(\frac{2\pi}{\lambda_E}L_{j+1} - \omega_E\tau\right) = \cos\left\{\frac{2\pi}{\lambda_E}(L_j + 2l) - \omega_E\tau\right\} = \cos\left\{\left(\frac{2\pi}{\lambda_E}L_j - \omega_E\tau\right) + \frac{2\pi}{\lambda_E}2l\right\}. \tag{21}$$

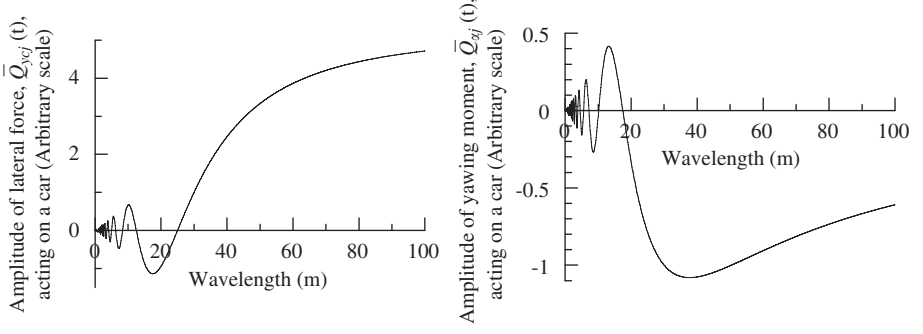


Fig. 10. Amplitudes of lateral force, $\overline{Q}_{y_{cj}(t)}$, and yawing moment, $\overline{Q}_{\alpha_j}(t)$ acting on Car $j$ in the train. See Eqs. (17) and (19).

Table 2
System parameters for a finite-length train in a tunnel

| | | |
|---|---|---|
| $N = 5$ | $2l_j(= l_{car}) = 14.12$ (25 m) | $L_A = 70.6$ (125 m) |
| $a = 1.77$ m | $\beta = 0.72$ | $R^*/a = 2.24$ |
| $A/A_d = 0.2$ | $A'/A = 1.0$ | $\rho_f = 1.23\,\mathrm{kg/m^3}$ |
| $\rho_{car} = 151.6\,\mathrm{kg/m^3}$ | $U = 5.0$ (= 102.3 m/s = 368 km/h) | $C_N = 0.00644$ |
| $C_T = 2C_N = 0.01288$ | $C_D = 0$ | $C_b = 0.157$ |
| $f_n = 1.0$ | $f_t = 0.8$ | $C_E = 0.06$ |
| St = 0.1 | $k_f = k_b = 3.53 \times 10^5\,\mathrm{N/m}$ $(= k_0)$ | $k_\alpha = 3.0 \times 10^7\,\mathrm{N\,m/rad}$ |
| $k_\eta = 9.8 \times 10^3\,\mathrm{N/m}$ | $c_f = c_b = 7.66 \times 10^4\,\mathrm{N\,s/m}$ | $c_\alpha = 0\,\mathrm{N\,m\,s/rad}$ |
| $c_\eta = 0\,\mathrm{N\,s/m}$ | | |

Because the phase expression in Eq. (16) is the same as that in Eq. (18), Eq. (21) also gives an indication of the phase relating the yawing moment between adjacent cars. This equation indicates that both the lateral force and the yawing moment acting on the front car, Car $j$, lead the back car, Car $j+1$, by the phase difference $(2\pi/\lambda_E)2l$. For this reason, the front car, Car $j$, is expected to move first in the lateral and rotational directions, and then, after a phase interval of $(2\pi/\lambda_E)2l$, the back car, Car $j+1$ will move.

### 3.2. Solution of the equations of motion

The equations of motion are solved by the Runge–Kutta method. The dimensionless linearized equations of motion for the system subjected to a travelling aerodynamic force $F_{EX}(t)$ are written in matrix form as

$$[M]\left\{\begin{matrix}\ddot{y}\\ \ddot{\alpha}\end{matrix}\right\} + [C]\left\{\begin{matrix}\dot{y}\\ \dot{\alpha}\end{matrix}\right\} + [K]\left\{\begin{matrix}y\\ \alpha\end{matrix}\right\} = \{F_{EX}(t)\}, \tag{22}$$

where $[M]$ is the mass matrix, $[C]$ the damping matrix, and $[K]$ the stiffness matrix, $\{y|\alpha\}^{\mathrm{T}} = \{y_1, \alpha_1, y_2, \alpha_2, \ldots, y_N, \alpha_N\}^{\mathrm{T}}$ is the vector of the generalized coordinates and $\{F_{EX}(t)\} = \{Q_{y_{c1}}, Q_{\alpha_1}, Q_{y_{c2}}, Q_{\alpha_2}, \ldots, Q_{y_{cN}}, Q_{\alpha_N}\}^{\mathrm{T}}$, which are given in Eqs. (16) and (18). Let the following square partitioned matrices be defined as

$$[B] = \begin{bmatrix}[0] & [M]\\ [M] & [C]\end{bmatrix}, \quad [E] = \begin{bmatrix}-[M] & [0]\\ [0] & [K]\end{bmatrix},$$

each matrix being of order $2N$; similarly, we define the vector $\{z\}$ and $\{F(t)\}$ as

$$\{z\} = \left\{\begin{matrix}\{\dot{y}|\dot{\alpha}\}\\ \{y|\alpha\}\end{matrix}\right\}, \quad \{F(t)\} = \left\{\begin{matrix}\{0\}\\ \{F_{EX}(t)\}\end{matrix}\right\}.$$

Then, equations of motion (22) may be written in the form

$$[B]\{\dot{z}\} + [E]\{z\} = \{F(t)\}. \tag{23}$$

Pre-multiplying Eq. (23) by $[B]^{-1}$ and defining $[B]^{-1}[E] = -[Y]$, Eq. (23) can be written as

$$\{\dot{z}\} = [Y]\{z\} + [B]^{-1}\{F(t)\} = \{f(\{z\}, t)\}. \tag{24}$$

Finally, the fourth-order Runge–Kutta method is applied to Eq. (24), and the time histories of the displacement and the velocity of the system are obtained. The convergence of this computation has been validated by employing different time increments, $\Delta t$; we employ $\Delta t = 0.01$ in the computation. Initial conditions of $y_{cj} = \alpha_j = \mathrm{d}y_{cj}/\mathrm{d}t = \mathrm{d}\alpha_j/\mathrm{d}t = 0$ or $\{z\} = \{0\}$ at $\tau = 0$ are assumed for all computations presented here.

### 3.3. Response to travelling forces with wavelengths of $\lambda_E^* = 17.5, 25, 30$, and 33.3 m

In Section 3.1.3, it was shown that for a wavelength of 17.5 m the yawing moment is zero, while the lateral force is zero for a wavelength of 25 m. Thus, in this section, first, the transient response to travelling aerodynamic forces with wavelengths of either 17.5 or 25 m are illustrated; and then, the transient response due to forces with wavelengths of 30 and 33.3 m is obtained; these are examples of typical wavelengths of the aerodynamic force acting on high-speed trains (Sakuma et al., 1998; Suzuki, 1999). The steady-state mode shapes of the train are also obtained for these

examples. Table 2 gives the system parameters employed in this section, which are typical of actual high-speed trains in Japan. The number of cars in the train is set at $N = 5$. (It has been confirmed that similar results can be obtained for other number of cars.)

Fig. 11 illustrates the response of the train to a travelling aerodynamic force with a wavelength of 17.5 m. As shown in Section 3.1.3, the aerodynamic moment for this wavelength is zero; hence, the expectation is that the angular displacement of the cars will be zero. Figs. 11(a) and (b) show the lateral translational displacements of the centre of all five cars; Fig. 11(b) shows the steady-state response from $t = 29$ to 30, and Fig. 11(c) gives the angular displacements of all five cars.

As seen in Fig. 11(a), from $t = 0$ to 20, transient responses are clearly observed for all five cars. Cars 1 and 3 move in the positive direction and Cars 2 and 5 in the negative direction. Eventually, all the cars reach a steady-state with a phase difference from each other. Note that the transient response of the cars is very large, an order of magnitude larger than in the steady-state. In fact, the amplitude of the transient response of actual trains may be smaller than that obtained here because of differences between the analytical model and real trains. In real trains, the aerodynamic force acts gradually on the cars, *one by one*, from the head toward the tail of the train *when entering a tunnel*. In contrast, in the present model we assumed that the aerodynamic force acts on *all cars simultaneously* at $t = 0$.

As seen in Fig. 11(b), the steady-state lateral translational displacement of each car has the same magnitude; however, there is a phase difference between the motion of the cars, which can be explained in the following way. In Section 3.1.3, it was shown that the front car, Car $j$, is expected to move first in the lateral and rotational directions, respectively, and then, after a phase interval $(2\pi/\lambda_E)2l$, the next car, Car $j+1$ will move. Substituting $\lambda_E^* = 17.5$ and $2l^* = 25$ into $(2\pi/\lambda_E^*)2l^*$, we have $(2\pi/17.5)25 \simeq 2\pi(1.43)$ rad. Thus, the front car, Car $j$, leads the next car, Car $j+1$, by $2\pi(1.43)$, which can be observed in Fig. 11(b). Note that, since $2\pi(1.43) = 2\pi(1 + 0.43)$, it appears that the phase difference between two adjacent cars is $0.43(2\pi)$, as illustrated in Fig. 11(b).

On the other hand, as seen in Fig. 11(c), the rotational motion is approximately zero for all time. Hence, cars subject to a travelling aerodynamic force of wavelength 17.5 m display almost pure translational motion, and no rotational motion. This confirms the expectation stated at the beginning of this section. Fig. 11(d) shows the train mode shape in its steady-state, confirming that translational motion is dominant for all cars. Remember that this result can be expected from Fig. 10, because the yawing moment for a wavelength of 17.5 m is zero, while the lateral force has a peak value.

Fig. 12 illustrates the response of the train to a travelling aerodynamic force with a wavelength of 25 m. In this case, the lateral aerodynamic force is zero, and so the expectation is that there will be no translational displacement. Fig. 12(a) shows lateral translational displacements of the centre of each of the five cars. Figs. 12(b) and (c) give angular displacements of the cars, and Fig. 12(c) shows the steady-state motion from $t = 29$ to 30.

As seen in Fig. 12(a), the transient lateral responses of all the cars $y_{cj}$ are considerably smaller than those for $\lambda_E^* = 17.5$ m shown in Fig. 11(a). On the other hand, as seen in Fig. 12(b), from $t = 0$ to 15, rotational responses are clearly observed for all cars. All cars move in the negative direction and then slightly in the positive direction. The large transient motion in the rotational direction damps out very quickly, leading to the steady-state solution shown in Fig. 12(c); in this case the five cars all move in-phase with each other. However, it may be considered that there is a phase difference between the motion of adjacent cars, which can be explained in the following way. Substituting $\lambda_E^* = 25$ and $2l^* = 25$ into $(2\pi/\lambda_E^*)2l^*$, we have $(2\pi/25)25 = 2\pi$. Thus, the front car, Car $j$, leads the next car, Car $j+1$, by $2\pi$, which means all cars move in the same way as shown in Fig. 12(c). Hence, it is shown that each car when subject to a travelling aerodynamic force of wavelength 25 m shows only rotational motion.

Fig. 12(d) shows the mode shape of the train for its steady-state response, confirming that rotational motion is dominant for all cars. Again, note that this result can be expected from Fig. 10, because the lateral force of 25 m wavelength is zero, while the yawing moment has a non-zero value.

Figs. 13(a) and (b) illustrate the response of the train in the lateral and rotational directions, respectively, to a travelling aerodynamic force with a wavelength of 30 m. As seen in Fig. 13, initially, transient responses are clearly observed for all cars in both directions. Eventually, the large transient response damps out and the resulting steady-state response is as shown in Figs. 13(c) and (d).

Following a similar procedure to that described earlier in this section, it can be shown that the steady-state responses of the cars are of the same magnitude but with a phase difference between their motions. The front car, Car $j$, leads the next car, Car $j+1$, by $2\pi(\frac{5}{6})$. Note that, since $2\pi(\frac{5}{6}) = 2\pi(1 - \frac{1}{6})$, it appears that the back car, Car $j+1$, leads the front car, Car $j$, by $\frac{1}{6}(2\pi)$ as illustrated in Figs. 13(c) and (d). In other words, the motion of the tail-end cars travels toward the head of the train as a wave, even though the force travels from the head of the train toward the tail.

Fig. 13(e) shows the translational and rotational steady-state response for Car 3. The translational displacement leads the rotational displacement by $\frac{1}{4}(2\pi)$ or 90°, which is expected for all cars, as discussed in Section 3.1.3.

Fig. 14 illustrates the mode shapes of train in its steady-state response every $\frac{1}{4}(2\pi)$ and $\frac{1}{6}(2\pi)$, respectively. As shown in Fig. 14(b), since the phase difference between two adjacent cars is $\frac{1}{6}(2\pi)$ in the steady-state, the motion of the tail-end

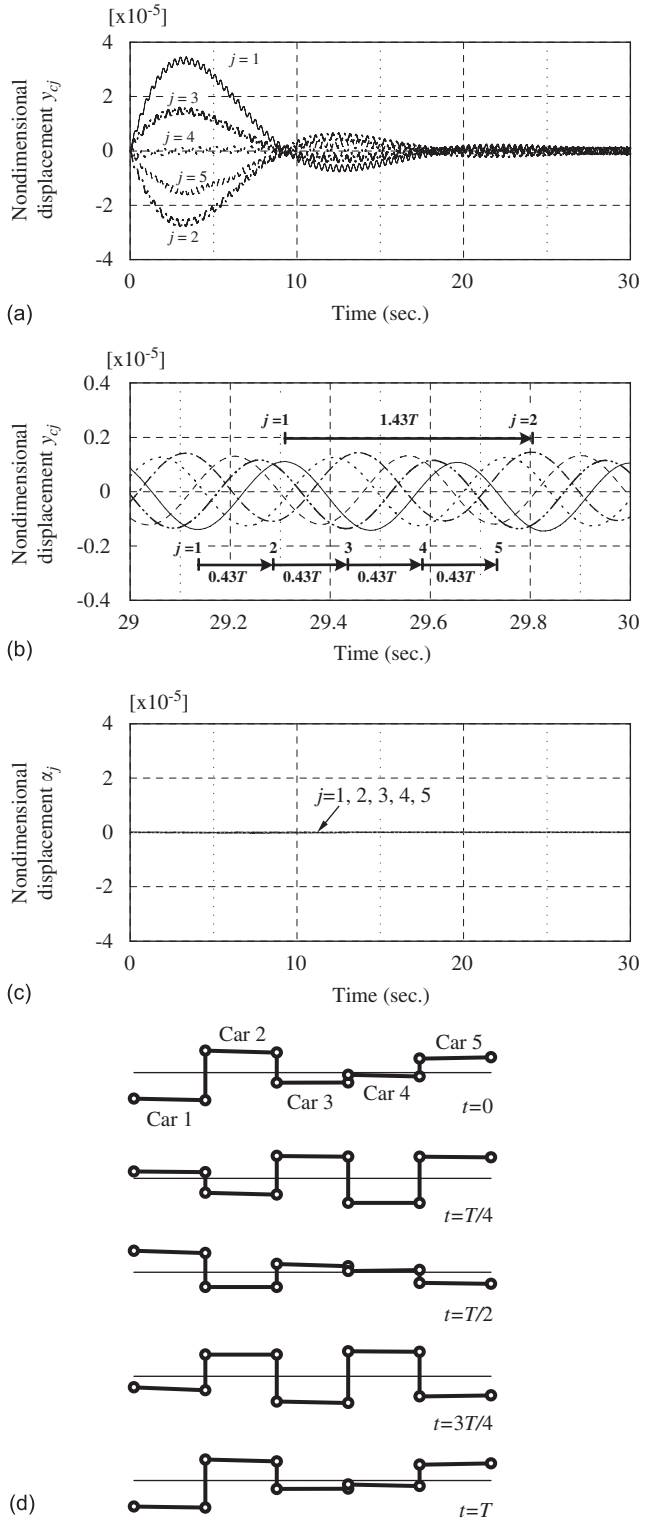


Fig. 11. Response to a travelling aerodynamic force with a wavelength of 17.5 m: ———, $j = 1$; — · —, $j = 2$; — · · —, $j = 3$; · · · · · · , $j = 4$; – – – , $j = 5$. (a) Translational response; (b) steady-state translational response ($t = 29-30$); (c) rotational response; (d) mode shape.

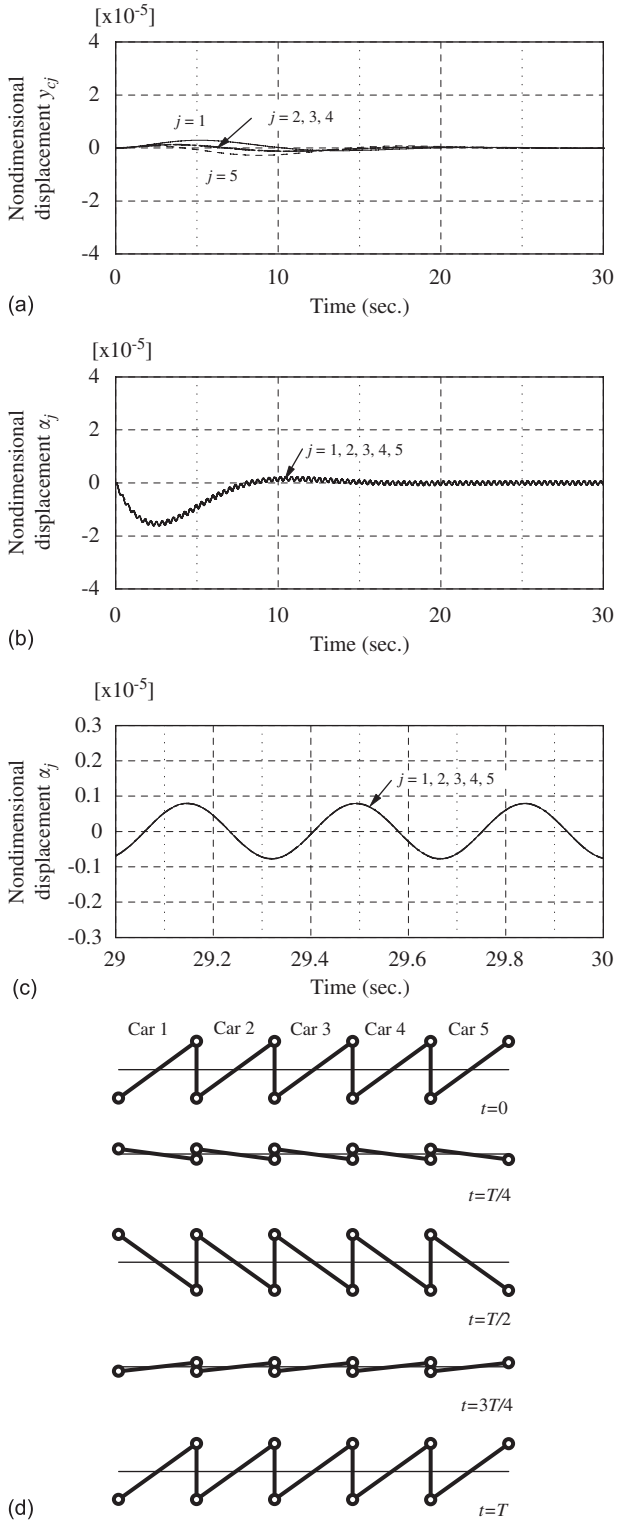


Fig. 12. Response to a travelling aerodynamic force with a wavelength of 25 m: ———, $j = 1$; — · —, $j = 2$; — · · —, $j = 3$; · · · · · · , $j = 4$; – – – , $j = 5$. (a) Translational response; (b) rotational response; (c) steady-state rotational response (($t = 29-30$); (d) mode shape.

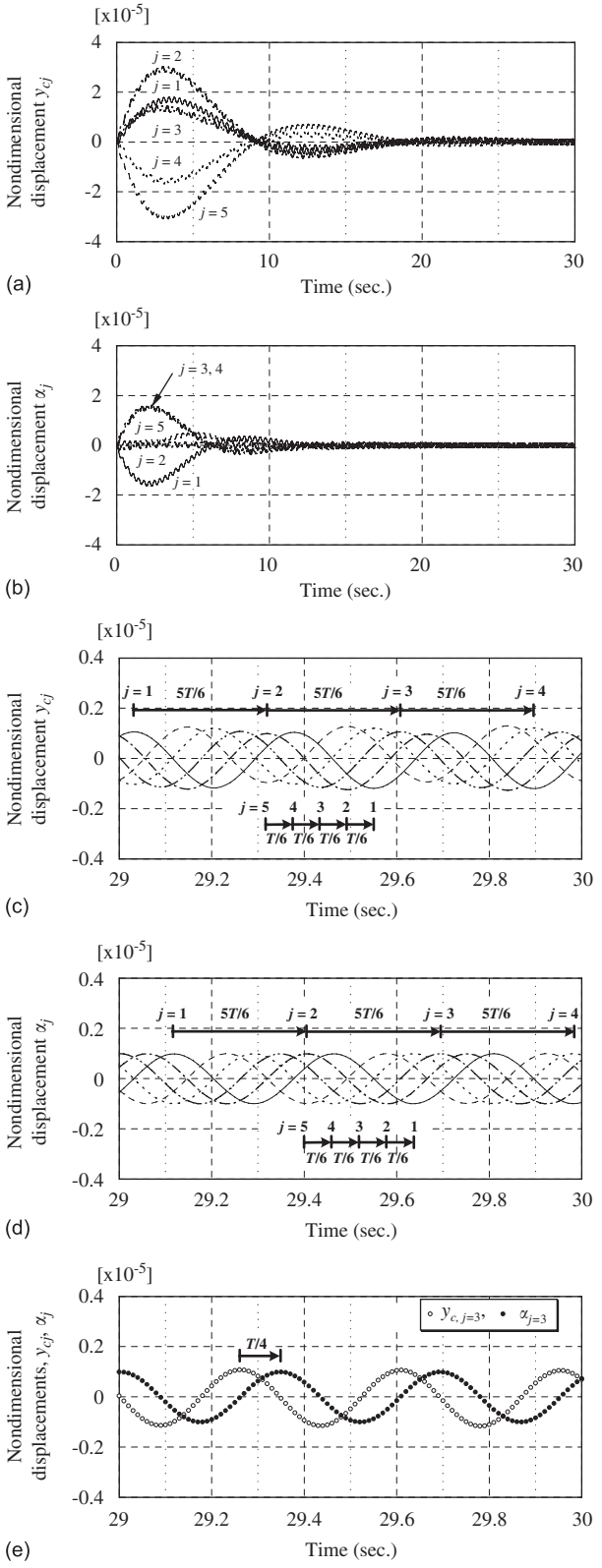


Fig. 13. Response to a travelling aerodynamic force with a wavelength of 30 m: ———, $j = 1$; — · —, $j = 2$; — · · —, $j = 3$; · · · · · · , $j = 4$; – – – , $j = 5$. (a) Translational response; (b) rotational response; (c) steady-state translational response ($t = 29-30$); (d) steady-state rotational response ($t = 29-30$); (e) translational and rotational steady-state response for Car 3 ($t = 29-30$).

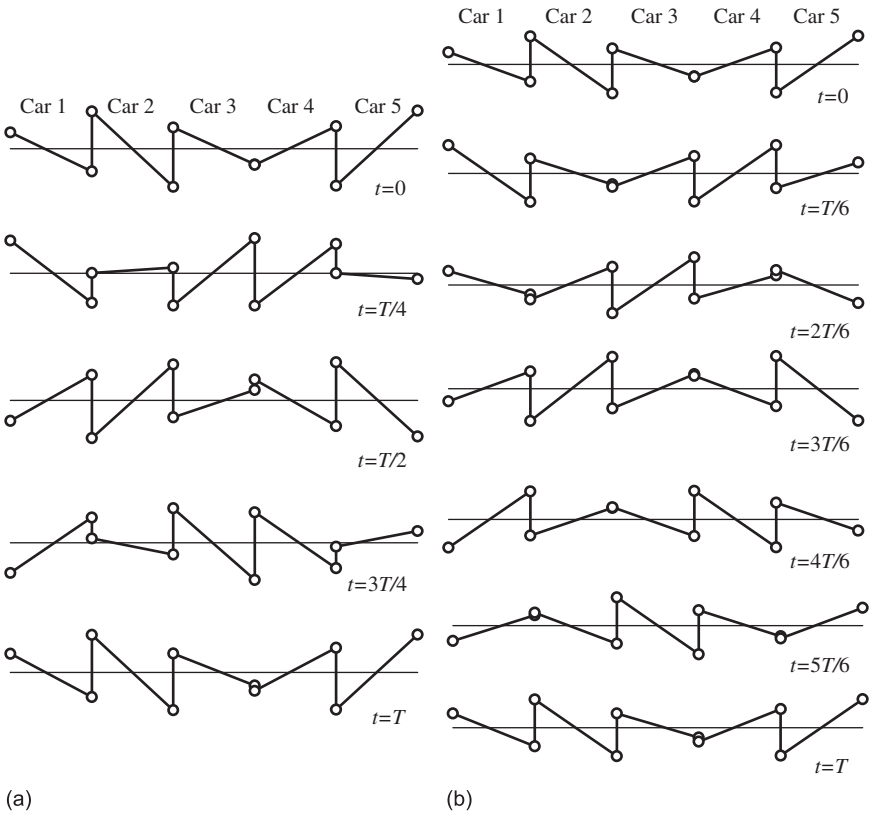


Fig. 14. Mode shape of the train in its steady-state response a travelling aerodynamic force with a wavelength of 30 m: (a) every $\frac{1}{4}(2\pi)$ and (b) every $\frac{1}{6}(2\pi)$.

cars can be considered to travel toward the head of the train as a wave, as mentioned before, even though the force travels from the head toward the tail of the train.

Figs. 15(a) and (b) show the response of the train in the lateral and rotational directions, respectively, to a travelling aerodynamic force with a wavelength of 33.3 m. Figs. 15(c) and (d) give enlarged views of, respectively, Figs. 15(a) and (b) in the steady-state for $t = 29-30$. As seen in Fig. 15, initially, transient responses of both $y_{cj}$ and $\alpha_j$ are clearly observed for all cars. Eventually, all the displacements fall within a range where the cars move with some phase difference to each other, which shows that the system has reached steady-state. As before, it is noted that the transient response of the cars is very large, an order of magnitude larger than the steady-state. As seen in Figs. 15(c) and (d), the displacements of each car behave in almost the same way, with some phase difference between them. Using a similar procedure as before, it can be shown that the front car, Car $j$, leads the back car, Car $j+1$, by $2\pi(\frac{3}{4})$, which can be observed in Figs. 15(c) and (d). Note that the motion of Car 1 and Car 5 are identical because of the phase difference $2\pi(\frac{3}{4})$. Since $2\pi(\frac{3}{4}) = 2\pi(1-\frac{1}{4})$, it appears that the back car, Car $j+1$, leads the front car, Car $j$, by $\frac{1}{4}(2\pi)$ as illustrated in Figs. 15(c) and (d).

Fig. 15(e) shows the steady-state response for Car 3. The translational displacement leads the rotational displacement by $\frac{1}{4}(2\pi)$ or 90°, which is expected for all cars as discussed in Section 3.1.3.

Fig. 16(a) illustrates the mode shape of the train in its steady-state every $\frac{1}{4}(2\pi)$, as shown; since the phase difference between two adjacent cars is $\frac{1}{4}(2\pi)$, the motion of the tail-end cars can be considered to travel toward the head of the train as a wave, even though the force travels from the head toward the tail of the train.

### 3.4. Comparison with previous work

The steady-state mode shapes obtained from the present study are compared to those of previous work obtained from running experiments. Figs. 16(b) and (c) illustrate the motion of five adjacent cars in a high-speed train in

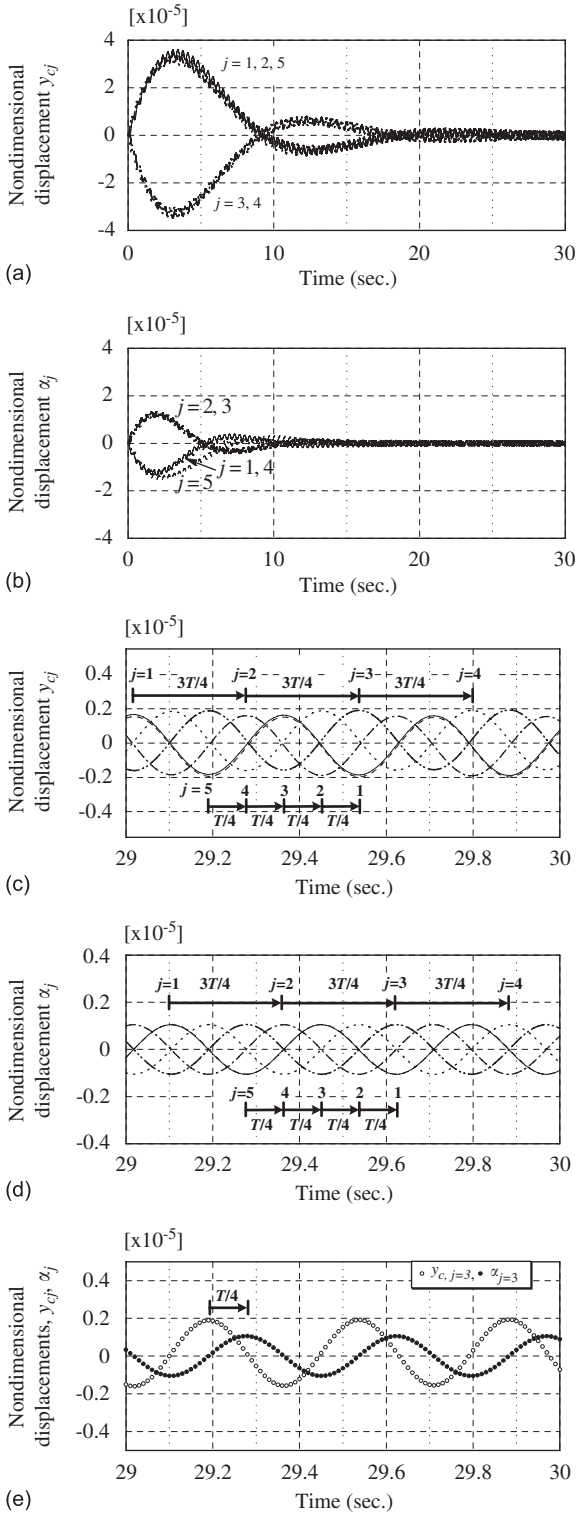


Fig. 15. Response to a travelling aerodynamic force with a wavelength of 33.3 m: ———, $j = 1$; — · —, $j = 2$; — · · —, $j = 3$; · · · · · · , $j = 4$; – – –, $j = 5$. (a) Translational response; (b) rotational response; (c) steady-state translational response ($t = 29-30$); (d) steady-state rotational response ($t = 29-30$); (e) translational and rotational steady-state response for Car 3 ($t = 29-30$).

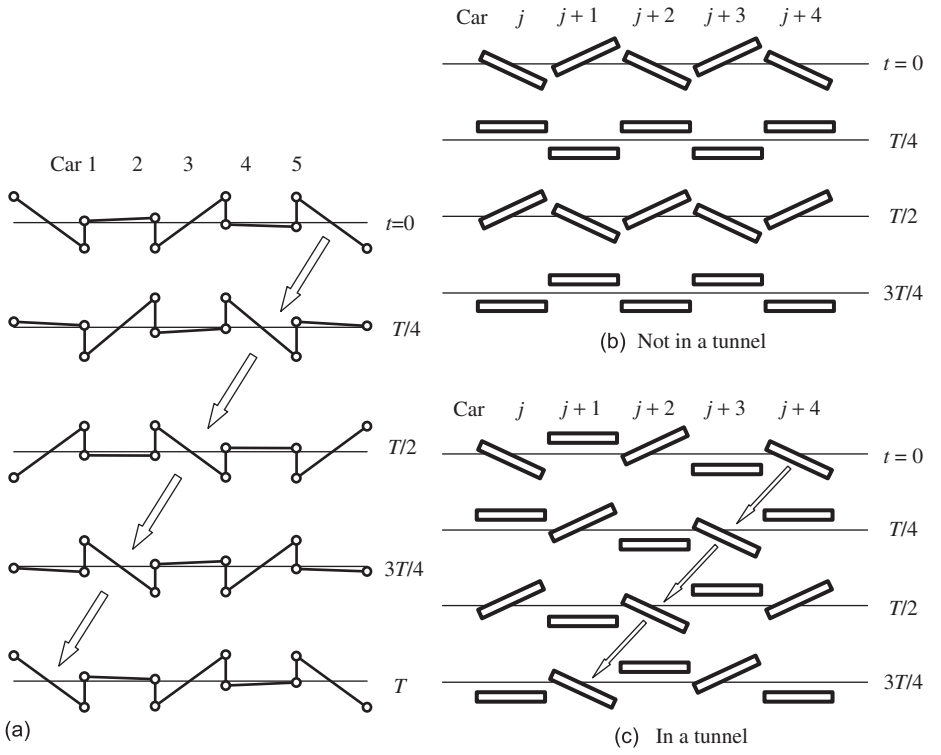


Fig. 16. (a) Mode shape of the train in its steady-state response to a travelling aerodynamic force with a wavelength of 33.3 m. (b), (c) Schematic drawing of the motion of five adjacent cars in a high-speed train: (b) in unconfined flow (no-tunnel), and (c) in tunnel sections *obtained from running experiments* (Fujimoto et al., 1998).

unconfined flow (no-tunnel) and in tunnel sections, respectively, obtained from running experiments by Fujimoto et al. (1998).

The mode shapes of a real train in unconfined flow (no-tunnel) are very different to those obtained when the train is in tunnel section. Compare the result for $t = 0$ in Fig. 16(a) and $t = 0$ in Fig. 16(c); also $t = T/4$ in Fig. 16(a) and $t = T/4$ in Fig. 16(c), *et seq*. From these comparisons, it is apparent that agreement between the results of the present numerical study and previous experiments in a tunnel section is good. Therefore, it is shown that the effect of the wavelength of a travelling aerodynamic force on the mode shapes of the finite-length train in the tunnel is considerable, and thus the wavelength controls the phase differences between cars in the train. This result reinforces the idea that the main cause of the vibrations of actual high-speed trains passing through tunnels is the forced vibrations induced by the travelling aerodynamic force along the train.

### 3.5. *Response to a force moving at the minimum phase velocity of a travelling wave in the train*

As mentioned previously, it is known that, when the travelling velocity of a sinusoidal aerodynamic force along a structure approaches the minimum phase velocity of travelling waves in the structure, the amplitude of the response increases (Mead, 1971; Manabe, 2002). Thus, in this subsection, the response of the present system is examined when the velocity of the moving force approaches that of the minimum phase velocity of a travelling wave in the system. In Section 2, free wave propagation in an infinite-length train was studied. It was shown in Fig. 3 that the minimum phase velocity of a travelling wave was approximately $\simeq 37$ m/s. Hence, the response of the present system is analyzed when the travelling force speed $V_E$ is set at this minimum phase velocity, i.e., $V_E = 37$ m/s. In addition, the response to the force moving at a velocity other than this minimum phase velocity is obtained. The system parameters employed in these calculations are as indicated in Table 3. Fig. 17(a) shows the response of Car 3 in a five-car train when the train is subjected to an aerodynamic force travelling with a velocity of 37 m/s. It is apparent from Fig. 17(a) that the amplitude of car displacements greatly increases with time. Fig. 17(b) illustrates the response to the force travelling at $V_E = 90$ m/s, and it is obvious that it is considerably smaller than that for $V_E = 37$ m/s.

Table 3
System parameters for analyzing the response of the finite-length train to the travelling aerodynamic force

| | | |
|---|---|---|
| $N = 5$ | $2l_j(= l_{\text{car}}) = 14.12$ (25 m) | $L_A = 70.6$ (125 m) |
| $a = 1.77\,\text{m}$ | $\beta = 0.72$ | $R^*/a = 2.24$ |
| $A/A_d = 0.2$ | $A'/A = 1.0$ | $\rho_f = 1.23\,\text{kg/m}^3$ |
| $\rho_{\text{car}} = 151.6\,\text{kg/m}^3$ | $U = 5.0$ (= 102.3 m/s = 368 km/h) | $C_N = 0.00644$ |
| $C_T = 2C_N = 0.01288$ | $C_D = 0.0$ | $C_b = 0.157$ |
| $f_n = 1.0$ | $f_t = 0.8$ | $C_E = 0.06$ |
| $\lambda_E^* = 100\,\text{m}$ | $k_f = k_b = 3.53 \times 10^5\,\text{N/m}$ | $k_\alpha = 3.0 \times 10^7\,\text{N m/rad}$ |
| $k_\eta = 9.8 \times 10^3\,\text{N/m}$ | $k_0 = 1.0 \times 10^4\,\text{N/m}$ | No mechanical damping |

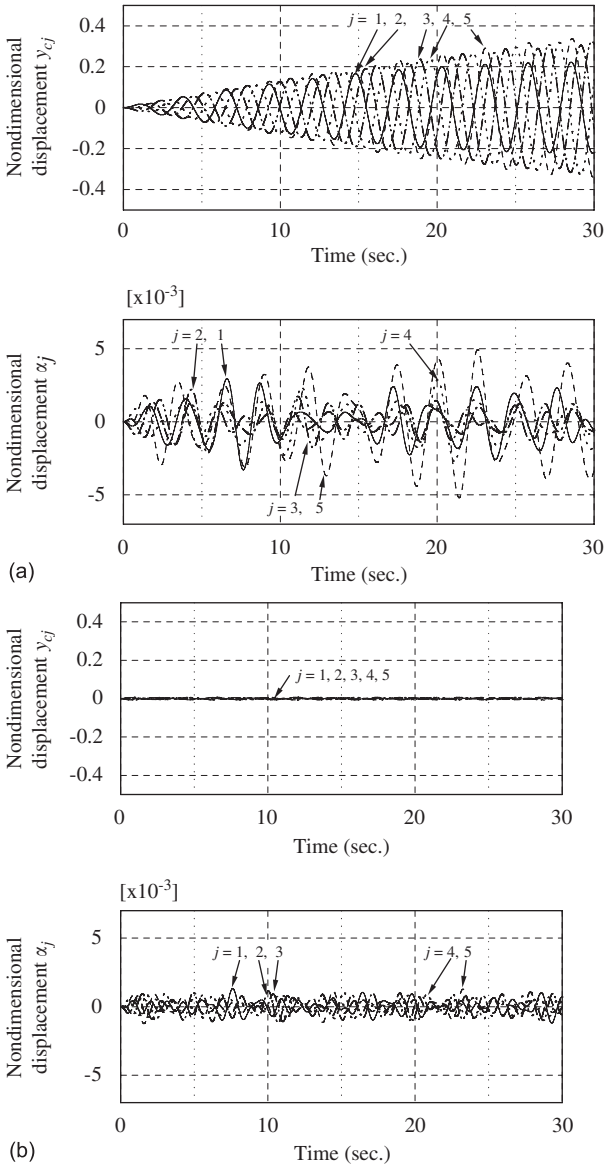


Fig. 17. Response to an aerodynamic force travelling (a) at the minimum phase velocity of travelling wave, $c_{ph}$, obtained in Section 2: $V_E = c_{ph} = 37\,\text{m/s}$ and (b) at $V_E = 90\,\text{m/s}$: ———, $j = 1$; — · —, $j = 2$; — · · —, $j = 3$; · · · · · ·, $j = 4$; – – –, $j = 5$. See Table 3 for values of system parameters employed.

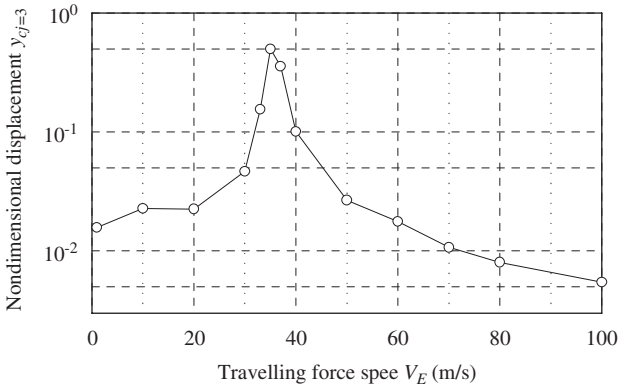


Fig. 18. Maximum lateral translational displacement response of the centre of Car 3 in a five-car train to a travelling aerodynamic force with speeds ranging from 0.01 to 100 m/s. See Table 3 for values of system parameters employed.

Finally, Fig. 18 shows the maximum lateral translational displacement response to a travelling force with speeds ranging from 0.01 to 100 m/s. The amplitude of the response to the force is a maximum for waves travelling at $V_E \simeq c_{ph,\min}$, and this maximum is considerably larger than that for the other travelling wave speeds. In fact, the maximum velocities of modern high-speed trains are in the range 50–100 m/s, which is higher than the minimum phase velocity of travelling wave, $c_{ph,\min} \simeq 37$ m/s, obtained in Section 2.

## 4. Conclusions

In Part 1, the companion paper to this one (Sakuma et al., 2008), modelling and basic dynamics of a train of flexibly interconnected rigid cylinders subjected to fluid dynamic forces were studied theoretically; in Part 2, this paper, wave propagation and response of the train system were examined.

The effect of aerodynamic forces and of the magnitude of translational, rotational, and supporting springs on wave propagation in an infinite-length train was examined in the present paper, both qualitatively and quantitatively, by considering the dispersion relations of the system. The following conclusions were obtained: (a) when fluid damping terms exist in the equations of motion, the frequency bands of the dispersion relation shift, and thus travelling wave modes may exist in the train, and (b) the effect of aerodynamic forces on wave propagation in a train with bogie cars ($\beta = 0.72$) is greater than that for a train of articulated cars ($\beta = 1.0$), especially in the transverse mode.

The response of the LTB finite-length train to a travelling sinusoidal aerodynamic force was also examined, as this simulates the features of the force experienced by trains passing through a tunnel. In addition, the response of the system was examined when the velocity of the force approached that of the minimum phase velocity of travelling waves in the system.

The effects of the wavelength, $\lambda_E$, of the travelling aerodynamic force on the mode shapes of a finite-length train were clarified. It was shown that the wavelength controls the phase differences between cars in the train. The front car moves first in the lateral and rotational directions, and then after a phase interval given by $(2\pi/\lambda_E)l_{\text{car}}$, the back car moves. Both the lateral force and yawing moment acting on the front car lead those on the back car by the same phase difference. For this reason, it appears that, for certain wavelengths, the steady-state motion of the tail-end cars can be considered to travel toward the head of the train as a wave, even though the force travels from the head of the train toward its tail.

The mode shapes obtained for the train in its steady-state are qualitatively in good agreement with those of previous work obtained in running experiments by Fujimoto et al. (1998). These results reinforce the idea that the vibration of actual high-speed trains running through tunnels is mainly forced vibration by the travelling aerodynamic force along the train. In addition, even though a large number of simplifying idealizations were introduced, especially in the structural model, the present model may be sufficient to examine qualitatively the response of a train to this aerodynamic force.

Finally, the response of a train to a force moving at the minimum phase velocity of travelling waves in the train was examined. It was found that the response of the train can be considerably amplified when the speed of the travelling force coincides with the minimum phase velocity of travelling waves in the train.

## References

Born, M., Hunag, K., 1954. Dynamical Theory of Crystal Lattices. Clarendon Press, Oxford.

Brillouin, L., 1946. Wave Propagation in Periodic Structures. McGraw Hill, New York.

Chen, S.S., Rosenberg, G.S., 1971. Vibrations and stability of a tube conveying fluid. Argonne National Laboratory Report ANL-7762, Argonne, IL, USA.

Fujimoto, H., 1999. Research on dynamic influences of vehicle coupling and vibration in running railway vehicles. Technical Report 29 (Special), Railway Technical Research Institute (in Japanese).

Fujimoto, H., Miyamoto, M., 1996. Lateral vibration and its decreasing measure of a shinkansen train. Vehicle System Dynamics Supplement 25, 188–199.

Fujimoto, H., Ueki, K., Suzuki, M., 1998. Lateral vibration modes and its decreasing measures in a high-speed train. In: Proceedings of the Joint Railway Technology Symposium (J-RAIL) '98, Tokyo, Japan, pp. 563–566.

Harrison, H.R., Nettleton, T., 1997. Advanced Engineering Dynamics. Wiley, New York.

Ishihara, T., Utsunomiya, M., Okumura, M., Sakuma, Y., Shimomura, T., 1997. An investigation of lateral vibration caused by aerodynamic continuous force on high-speed train running within tunnels. In: Proceedings of the World Congress on Railway Research '97, Florence, Italy, pp. 531–538.

Manabe, K., 2002. Tetsudo niokeru hadou to shindou (Wave and Vibration Problems in Railway System). Kotsushimbunsha (in Japanese).

Mead, D.J., 1971. Vibration response and wave propagation in periodic structures. ASME Journal of Engineering for Industry 93, 783–792.

Nakade, K., Suzuki, M., Fujimoto, H., 2004. Interaction between vehicle vibration and aerodynamic force on high-speed train running in tunnel. Vehicle System Dynamics Supplement 41, 717–723.

Païdoussis, M.P., 1986. Stability of a chain of cylinders travelling underwater. In: Proceedings of the 5th International Offshore Mechanics and Arctic Engineering Symposium, Tokyo, Japan, ASME, New York, pp. 483–490.

Païdoussis, M.P., 1998. Fluid–Structure Interactions: Slender Structures and Axial Flow, vol. 1. Academic Press, London.

Païdoussis, M.P., 2003. Fluid–Structure Interactions: Slender Structures and Axial Flow, vol. 2. Elsevier Academic Press, London.

Sakuma, Y., Suzuki, M., Maeda, T., 1998. Measurement of flow around a high-speed train. In: Proceedings of 4th KSME-JSME Fluids Engineering Conference, Pusan, Korea, pp. 177–180.

Sakuma, Y., Païdoussis, M.P., Price, S.J., 2008. Dynamics of trains and train-like articulated systems travelling in confined fluid. Part 1: Modelling and basic dynamics. Journal of Fluids and Structures 24, this issue, doi:10.1016/j.jfluidstructs.2008.01.002.

Sasaki, K., Shimomura, T., 1989. Improvement of riding comfort of the 0 series shinkansen. RTRI Report 3 (12), 10–17 (in Japanese).

Sawada, K., 2000. Railway technology today 12: Magnetic Levitation (MAGLEV) Technologies. Japan Railway & Transport Review 25.

Sugimoto, N., 1996. Aeroelastic stability of a beam travelling in a tunnel lined with resonators. AIAA Journal 34, 2005–2013.

Sugimoto, N., Kugo, K., Watanabe, Y., 2002. Derivation of nonlinear wave equation for flexural motions of an elastic beam travelling in an air-filled tube. Journal of Fluids and Structures 16, 597–612.

Suiker, A., Metrikine, A., de Borst, R., 2001. Dynamic behaviour of a layer of discrete particles, Part 2: response to a uniformly moving, harmonically vibrating load. Journal of Sound and Vibration 240, 19–39.

Suzuki, M., 1999. A model of aerodynamic force acting on train sides travelling in a tunnel. Technical Research Report of Railway Technical Research Institute (in Japanese).

Suzuki, M., 2001. Unsteady aerodynamic force acting on high speed trains in tunnel. Quarterly Report of RTRI 42 (2), 89–93.

Suzuki, M., Maeda, T., Arai, N., 1996. Numerical simulation of flow around a train. In: Deville, M., et al. (Eds.), Notes on Numerical Fluid Mechanics, vol. 53. Vieweg, Braunschweig, pp. 311–317.

Suzuki, M., Nakade, K., Fujimoto, H., 2001. Study on interaction between vehicle dynamics and aerodynamic force on high-speed train in tunnel. RTRI Report 15 (5), 19–24 (in Japanese).

Suzuki, M., Fujimoto, H., Sakuma, Y., 2002. Measures to reduce aerodynamic force acting on high-speed train in tunnel. In: Proceedings of the 11th Transportation and Logistics Conference (TRANSLOG 2002), Kawasaki, Japan, JSME, Tokyo, pp. 277–278 (in Japanese).

Takai, H., 1989. Maintenance of long-wave track irregularity on Shinkansen. RTRI Report 3 (4), 13–20 (in Japanese).

Ueki, K., Nakade, K., Fujimoto, H., 1999. Lateral vibration of middle cars of shinkansen train in tunnel section. Vehicle System Dynamics Supplement 33, 749–761.

Watanabe, Y., Sugimoto, N., 2003. Localized solutions to the nonlinear wave equation for flexural motions of an elastic beam traveling in an air-filled tube. Wave Motion 38, 295–309.

Watanabe, Y., Sugimoto, N., 2005. Flexural wave propagation in a spatially periodic structure of articulated beams. Wave Motion 42, 155–167.